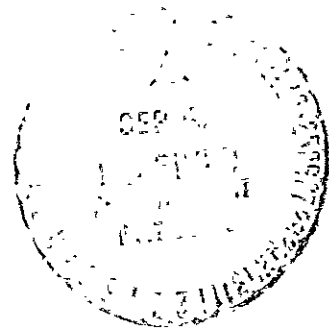


IITRI



FACILITY FORM 602

1 N70-37388	
(ACCESSION NUMBER)	(THRU)
61	1
(PAGES)	(CODE)
CR-102826	33
(NASA CR OR TMX OR AD NUMBER)	(CATEGORY)

CR-102826

Report No. IITRI-U6002-90
(Triannual Report)

DEVELOPMENT OF SPACE-STABLE
THERMAL-CONTROL COATINGS

National Aeronautics & Space Administration
George C. Marshall Space Flight Center
Huntsville, Alabama 35812

IIT RESEARCH INSTITUTE

Report No. IITRI-U6002-90
(Triannual Report)

DEVELOPMENT OF SPACE-STABLE
THERMAL-CONTROL COATINGS

January 1 through April 30, 1970

Contract No. NAS8-5379
Funded Under Code 124-09-18-05-04-25-8-004-028-2510
IITRI Project U6002

Prepared by
J.E. Gilligan
and
G.A. Zerlaut

of

IIT RESEARCH INSTITUTE
Technology Center
Chicago, Illinois 60616

for

National Aeronautics & Space Administration
George C. Marshall Space Flight Center
Huntsville, Alabama 35812

July 1, 1970

IIT RESEARCH INSTITUTE

FOREWORD

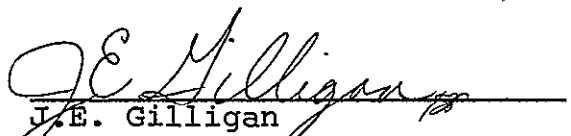
This is Report No. IITRI-U6002-90 (Triannual Report) of IITRI Project U6002, Contract No. NAS8-5379, entitled "Investigation of Environmental Effects on Coatings for Thermal Control of Large Space Vehicles." This report covers the period from January 1 through April 30, 1970. Previous Triannual Reports were issued on October 25, 1963; March 5, 1964; July 20, 1964; December 21, 1964; February 23, 1965; July 20, 1965; November 9, 1965; February 21, 1966; July 11, 1966; November 30, 1966; February 28, 1967; September 22, 1967; January 15, 1968; April 15, 1968; October 25, 1968; January 31, 1969; July 11, 1969; November 17, 1969; and February 20, 1970.

Major contributors to the program during this period include: Gene A. Zerlaut, Project Leader; Dr. Samuel I. Baker, experimental and theoretical studies pertaining to characterization of proton accelerator (CREF); Mr. Robert F. Boutin, experimental work on CREF; Mr. John E. Gilligan, group responsibility for CREF and analytical studies pertaining to its characterization; and, Mr. George Kimura, experimental work.

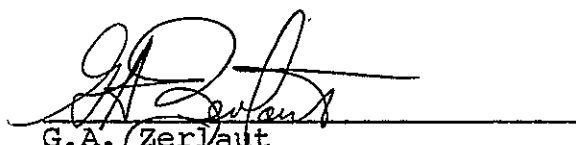
The work reported herein was performed under the technical direction of the Space Sciences Laboratory of the George C. Marshall Space Flight Center; Mr. Daniel W. Gates acted as the Project Manager.

Prior to March 15, 1966, this contract was funded under Codes 124-09-05-26-04, 124-09-05-00-14, 933-50-01-00-00 and 908-20-02-01-47.

Respectfully submitted,
IIT RESEARCH INSTITUTE


J.E. Gilligan
Group Leader-Thermal Control
Polymer Chemistry Research

APPROVED:


G.A. Zerlaut
Manager
Polymer Chemistry Research

JEG:jss

IIT RESEARCH INSTITUTE

ABSTRACT

The concept, design, construction, characterization and performance of the solar wind-proton simulation facility, designated Combined Radiation Environment Facility (CREF), is described in this report. The CREF consists of three modules, one of which, the space-ultraviolet simulator, is not physically coupled to the other two. The proton accelerator (solar wind simulator) is physically coupled to the basic IRIF-II facility, the vacuum system that provides for sample manipulation, irradiation and in situ hemispherical spectral reflectance measurement. Performance objectives are all either met or exceeded.

TABLE OF CONTENTS

	<u>Page</u>
FOREWORD	iii
ABSTRACT	iv
LIST OF FIGURES	vi
I.. INTRODUCTION	1
II. DESIGN, PERFORMANCE CRITERIA AND CHARACTERIZA- TION OF CREF	3
A. General Introduction	3
B. Space Simulation Criteria - A Discussion	20
C. Performance	26
III. RESULTS OF PROTON (SOLAR-WIND) IRRADIATION	38
A. Test Conditions	38
B. Results	38
C. Discussion	46
IV. CONCLUSIONS	47
REFERENCES	49
APPENDIX - CALCULATION OF BENDING	

LIST OF FIGURES

<u>Figure No.</u>		<u>Page</u>
1	THE COMBINED RADIATION ENVIRONMENT TEST FACILITY (CREF)	5
2	CLOSE-UP OF THE CREF	6
3	CLOSE-UP OF THE CREF SHOWING THE IRIF AND THE SAMPLES (REFLECTED IN THE 45° MIRROR)	7
4	COMBINED RADIATION ENVIRONMENT FACILITY	8
5	BLOCK DIAGRAM OF PRESENT CREF FACILITY	9
6	PROTON SOURCE, EXTRACTOR LENS AND 1st EINZEL LENS	11
7	TWO-ELEMENT EXTRACTOR LENS (DISASSEMBLED) TO REDUCE FLUX FROM RF SOURCE	12
8	EINZEL LENSES; TWO VIEWS	13
9	45° BEND (FOR MAGNET) AND FARADAY-CUP HOUSING	14
10	MASS SEPARATOR AND MASS ANALYZER (SHOWING SECOND EINZEL LENS)	15
11	FARADAY CUP FLUX MAPPER	16
12	EJECTION LENS (SWEEP/COLLIMATOR)	18
13	MAGNETIC ANALYSIS AND PHYSICAL ISOLATION OF PROTON BEAM	25
14	ION CURRENT VS MAGNETIC FIELD STRENGTH, GAUSS (B-SCAN)	29
15	23-ELEMENT FARADAY CUP FOR BEAM MAPPING AT SAMPLE LOCATION	31
16	FLUX INTENSITY AT SAMPLE LOCATION VS COLLIMATOR LENS POTENTIAL	33
17	FLUX INTENSITY MAP AT SAMPLE LOCATION (SCALE 1:1)	34
18	PROTON CURRENT VS SUPPRESSOR VOLTAGE	35
19	PLASMA CURRENT VS APPLIED POTENTIAL	36

<u>Figure No.</u>		<u>Page</u>
20	EFFECT OF 2.5×10^{15} PROTONS/CM ² ON IN SITU REFLECTANCE SPECTRA OF SP500 ZINC OXIDE	39
21	EFFECT OF 2.7×10^{15} PROTONS/CM ² ON IN SITU REFLECTANCE SPECTRA OF Z93 THERMAL-CONTROL PAINT	40
22	EFFECT OF 2.5×10^{15} PROTONS/CM ² ON IN SITU REFLECTANCE SPECTRA OF S-13G THERMAL-CONTROL PAINT	41
23	EFFECT OF 2.7×10^{15} PROTONS/CM ² ON IN SITU REFLECTANCE SPECTRA OF PLASMA-CALCINED Zn ₂ TiO ₄	42
24	EFFECT OF 2.7×10^{15} PROTONS/CM ² ON IN SITU REFLECTANCE SPECTRA OF PS7 PAINT PIGMENTED WITH ACID PHOSPHATE-TREATED Zn ₂ TiO ₄	43
25	EFFECT OF 2.5×10^{15} PROTONS/CM ² ON IN SITU REFLECTANCE SPECTRA OF OWENS ILLINOIS 650 (SILICONE) PAINT PIGMENTED WITH CYANATED Zn ₂ TiO ₄	44
A-1	MAGNETIC FIELD PROFILE	A-4

Report No. IITRI-U6002-90
(Triannual Report)

DEVELOPMENT OF SPACE-STABLE THERMAL-CONTROL COATINGS

I. INTRODUCTION

The general requirement under this contract is the development of thermal-control surface coatings that possess very low but stable ratios of solar absorptance (α_s) to infrared emittance (ϵ_h). Historically, this program has been divided into three major phases: (1) inorganic pigment technology, (2) silicone-photolysis and silicone-paint investigations, and (3) general coatings investigations.

The relative emphasis on each major task has varied during the course of the program according to the urgency of the various problems elucidated by our investigations as well as the availability of both funds and personnel. The major emphasis during the past two years has involved the investigation of new, potentially stable white-pigments - particularly zinc orthotitanate- and the design and construction of a combined-environment radiation facility (CREF).

The studies reported in the last Triannual Report (IITRI-U6002-85) included the results of the in situ optical spectroscopy of ultraviolet-irradiated, reactively encapsulated (surface treated) zinc orthotitanates (Zn_2TiO_4). The data were compiled and, in conjunction with the results of electron paramagnetic resonance (epr) spectroscopy presented previously, the effects of various treatments were evaluated. These studies showed that the single most important factor in achieving optical stability with Zn_2TiO_4 is the employment of excess (~0.5%) ZnO in the preparative reaction. Still of significance, however, but of secondary importance, are surface treatments such as plasma annealing and reaction with potassium silicate. We know from previous studies that residual ZnO must be present when any

high-temperature heat treating is performed. Of the reactive surface treatments, silicating (and preparation of potassium silicate-based coatings) is the most effective in improving stability of Zn_2TiO_4 .

Although considerable studies of surface-treated zinc ortho-titanate pigment and pigmented coatings were performed during the report period, as well as new pigment studies, this triannual report is being devoted to the design, construction, operation, characterization and performance of the low-energy proton accelerator module of the CREF space simulator. The materials studies enumerated above are the subject of a Triannual Report now in preparation.

The proton accelerator (solar wind simulator) portion of the CREF was conceived, designed and characterized with funds from this contract -- NAS8-5379, IITRI Project No. U6002. The proton accelerator and the IRIF-II module, and all ancillary electronic and vacuum facilities, were constructed, assembled and de-bugged employing in-house funds furnished by IIT Research Institute.

II. DESIGN, PERFORMANCE CRITERIA AND CHARACTERIZATION OF CREF

A. General Introduction

1. Background

For approximately ten years researchers in the field of spacecraft temperature control materials have been attempting to develop materials whose optical properties are unaffected by the hostile elements of the space environment. During this period we have learned much about the manner in which we should test candidate materials. Nevertheless, it was not until 4 years ago (Ref.'s 1, 2) that the need for in-situ testing was clearly demonstrated. Realizing this need, IITRI designed IRIF, the In-situ Reflectance Irradiation Facility (Ref. 3). As more sophisticated missions were considered and as spacecraft missions to the moon and planets became more common, the requirements of these missions for stable spacecraft thermal control materials became more demanding. The solar wind environment had to be added to the testing scheme, because the environment of deep space includes not only solar electromagnetic radiation but also solar wind protons.

There are two points which experience makes us think are highly important in the evolution of a simulation laboratory and the policy under which it operates. First, we firmly believe that responsible testing requires a materials science approach to the R&D of thermal control materials, a basic knowledge of the effects of ionizing radiations on materials, and an understanding of the operating principles and characteristics of the systems employed. Second, we recognize the need for credible simulation criteria. The greatest need we have at present in this sense is to assess the effects of non-simulation - the differences in effects on materials when compositions, flux rates and/or spectral flux rates are not close to space values.

IITRI's Combined Radiation Environment Facility, CREF, evolved after consideration of the above and many other points. A definite need exists for determining the effects of the deep space environment, where the solar wind and solar ultraviolet radiation are concurrent. Since these two types of radiation are fundamentally different - one massive and the other electromagnetic, we expect, therefore, that the mechanisms of their interactions will be fundamentally different.

2. Facility Description

The Combined Radiation Environment Facility (CREF) system has been described in a previous triannual report (Ref. 3). Photographs of the operational facility are presented in Figures 1 through 3. The components of this facility are shown schematically in Figure 4 and a block diagram is shown in Figure 5. Except for the ultraviolet irradiation facility (i.e., the burner and power supply), the entire integral simulation laboratory is shown in Figure 1. The Beckman DK-1 ultraviolet/visible spectrometer is shown to the rear (behind the CREF in the photograph); the control facilities, including the high-voltage divider, are shown in the left of the photograph. Figure 2 is a close-up of the operational proton accelerator and shows the interface with the IRIF, the basic in situ vacuum-irradiation facility, which has been described in the literature (Ref. 4). The IRIF and the interface with the accelerator are shown in Figure 3. The vacuum integrating sphere is shown on the left of this photograph. The 12 samples, mounted radially in the IRIF, are shown reflected in the 45° first surface mirror (located in the multiple-source adaptor housing) employed to direct ultraviolet down onto the samples; the proton-beam in the mirror is clearly shown.

Referring to Figures 1 through 4, let us describe the path of the protons in going from the ion source to the sample area. The protons are first generated in the RF (plasma) source at a potential of approximately 1200 volts. The flow of hydrogen

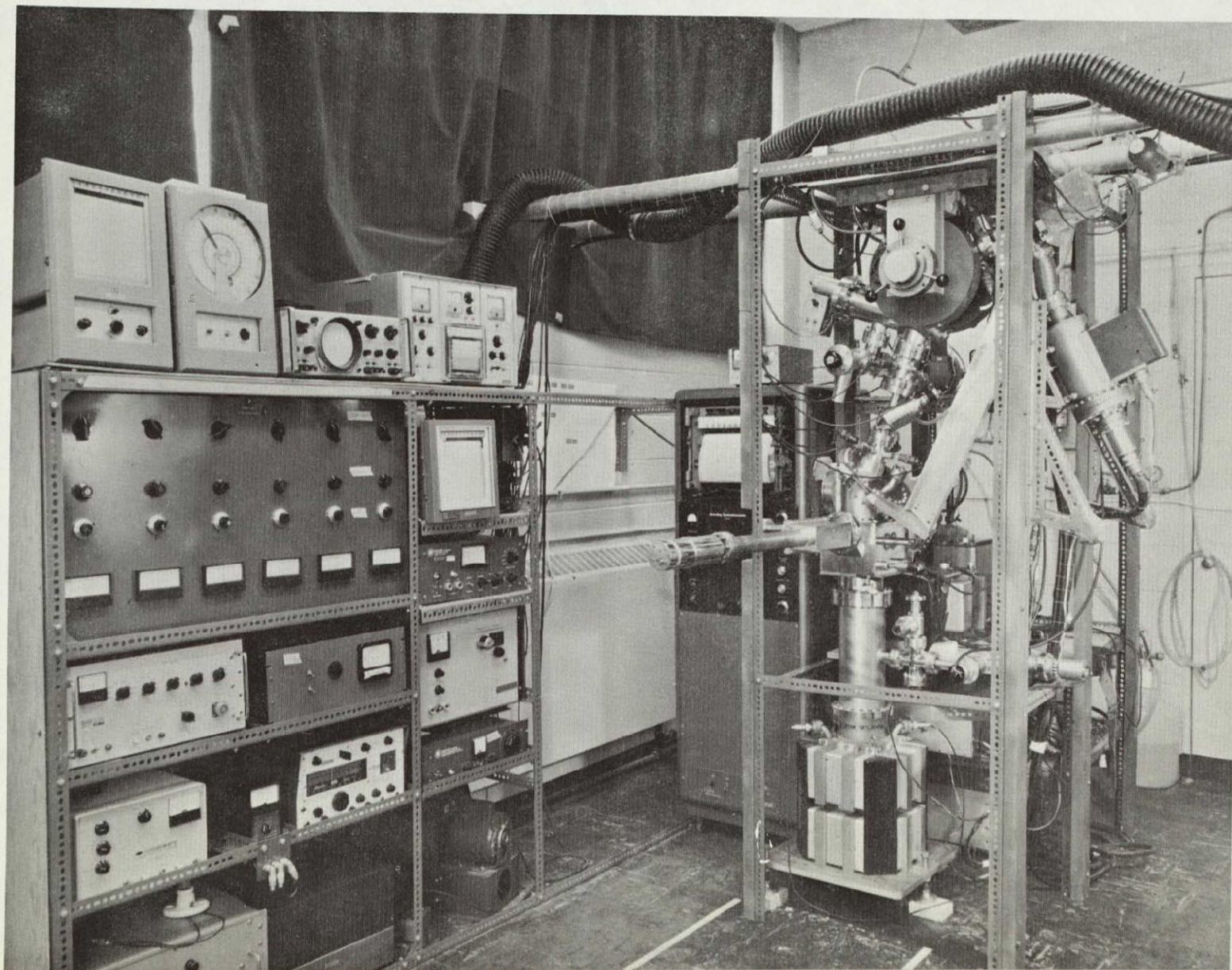


Figure 1 THE COMBINED RADIATION ENVIRONMENT TEST FACILITY (CREF)

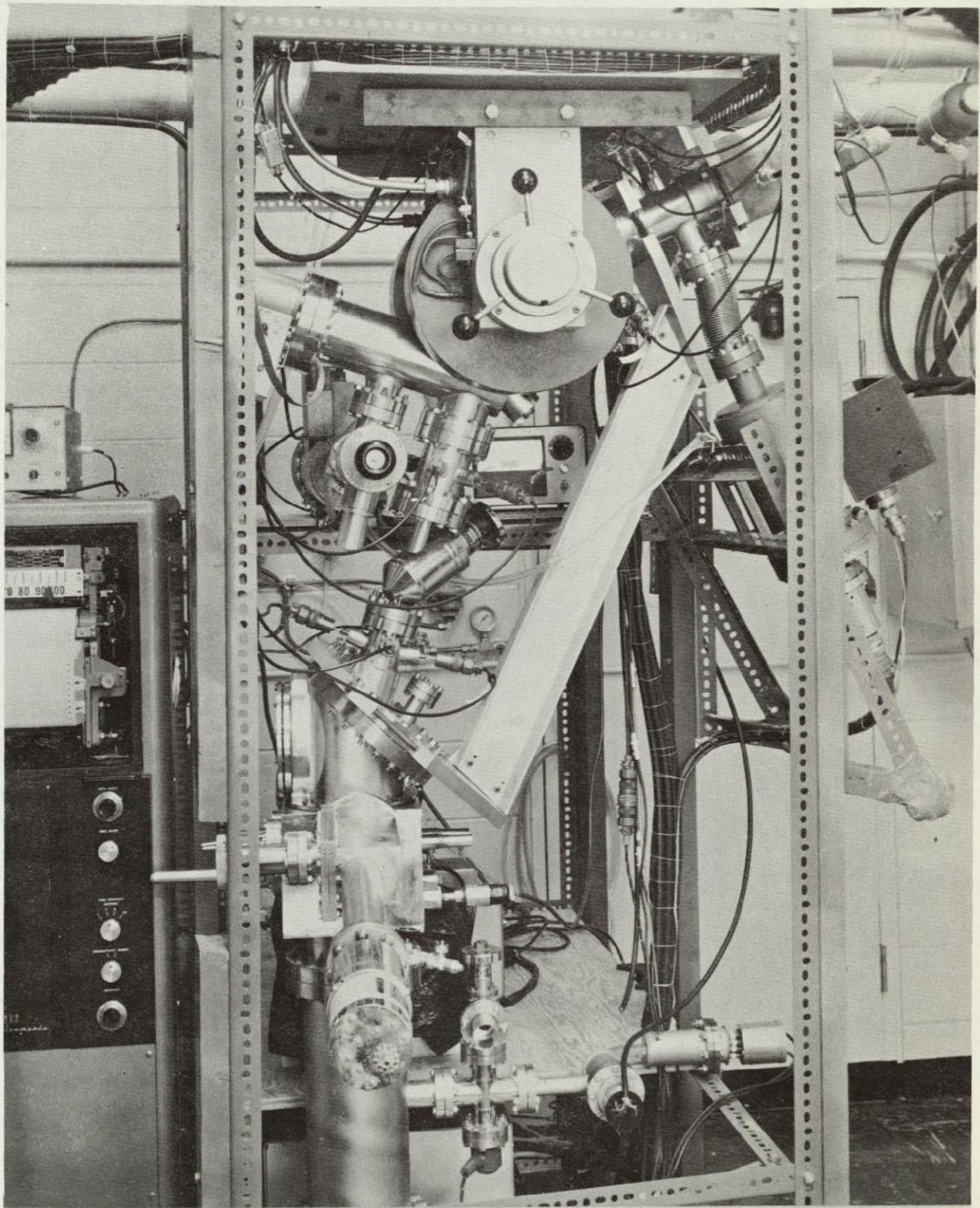


Figure 2 CLOSE-UP OF THE CREF

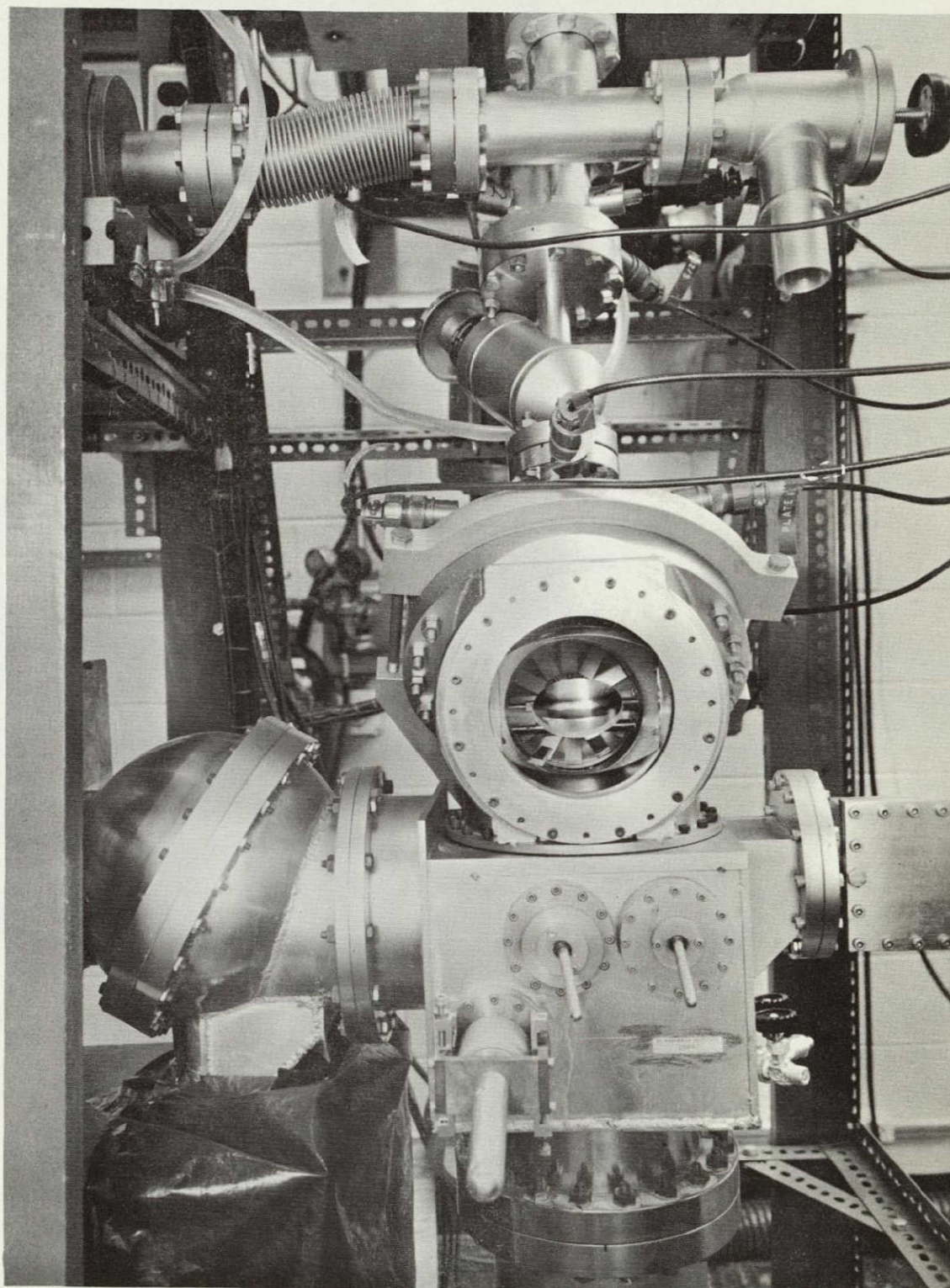


Figure 3 CLOSE-UP OF THE CREF SHOWING THE IRIF AND THE SAMPLES
(REFLECTED IN THE 45° MIRROR)

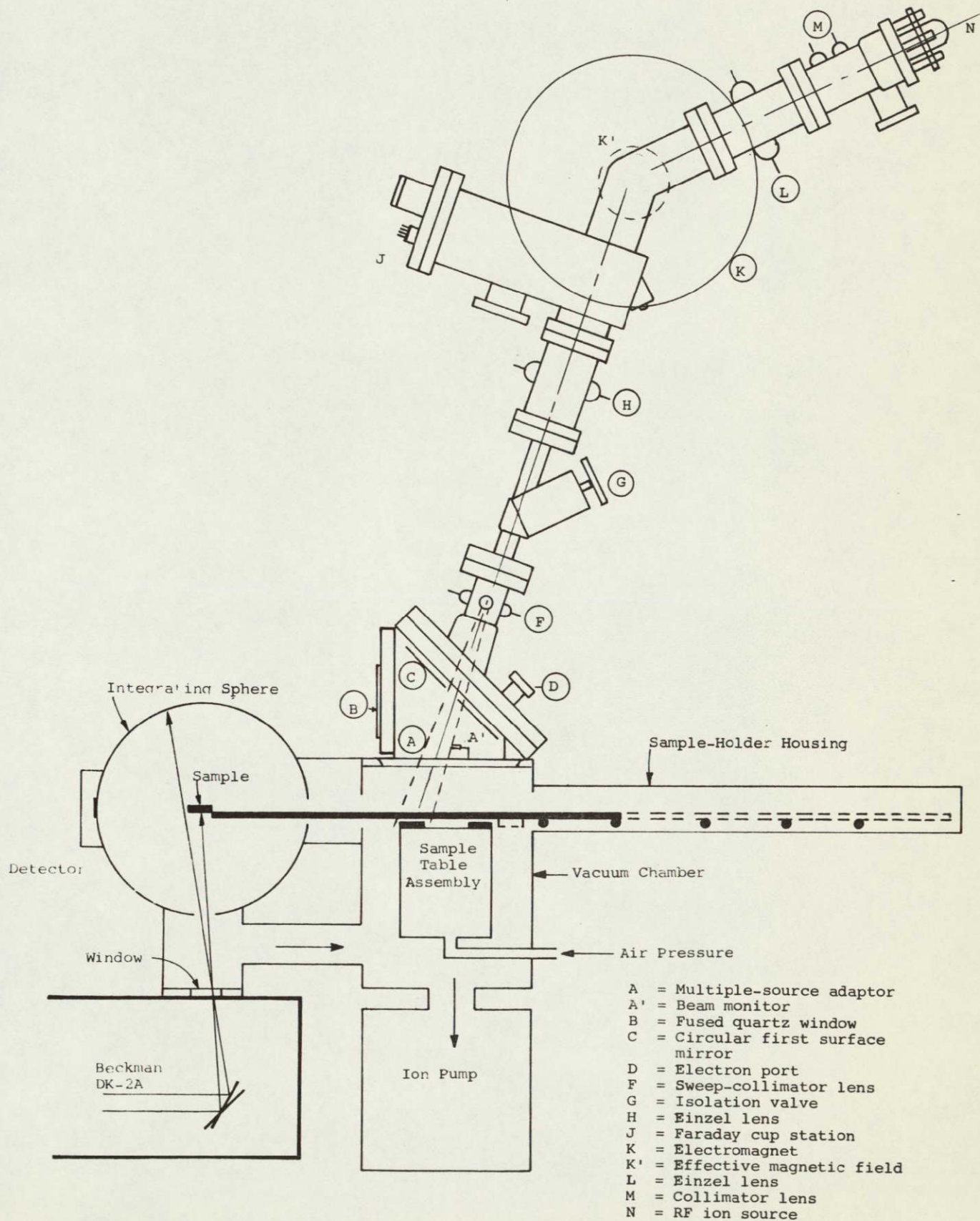


Figure 4 COMBINED RADIATION ENVIRONMENT FACILITY

into the glow discharge tube is controlled with a palladium leak. The source (and the extractor and first einzel lens) is shown in Figure 6; the copper RF-cage and RF-plates are removed to show the glow-discharge tube. (Alligator clamps are employed in this photo to identify the electrodes. The RF-cage is clearly shown in Figure 1.) The proton beam is extracted through a small hole in the RF source into the extractor region; two collimator lenses with small diameter holes reduce the beam current from the proton source, originally of the order of 175 microamps, to about 40 microamperes. The two electrodes controlling the extractor potential are shown in Figure 6; the disassembled extractor lens, showing the aperture, is shown in Figure 7. The extractor lenses also shape the beam, which then moves to the first einzel lens, which, in turn, focuses the beam into the magnet. The two einzel lenses, showing both views, are shown in Figure 8. The highly-regulated electromagnet is shown in Figure 6. The magnetic field applied by the magnet then selectively bends the ion components of the beam and thus physically separates the H^+ , H_2^+ and other species. The field strength is adjusted to obtain a 45° deflection of the H^+ beam, which focuses it into another einzel lens, which, in turn, focuses the beam (through a valve) into a quadrupole lens that then smoothes the beam out and produces a geometric flux-uniformity across the sample area. The disassembled 45° bend and the Faraday-Cup housing are shown in Figure 9. A Faraday Cup is located immediately downstream of the analyzer magnet and this is used to characterize the beam as it moves out of the magnet. The angular (geometric) separation, energy and uniformity of the beam can be determined with this cup. The Faraday Cup analyzer module, showing the magnetic chuck and the second einzel lens, is shown in Figure 10. The eight-element Faraday Cup detector and the magnetic chuck-driven positioning screw are shown in Figure 11. After final focusing in the second einzel lens, the beam passes through a valve unit and then into the quadrupole sweep/collimator lens. This element is shown in Figures 1 and 2,

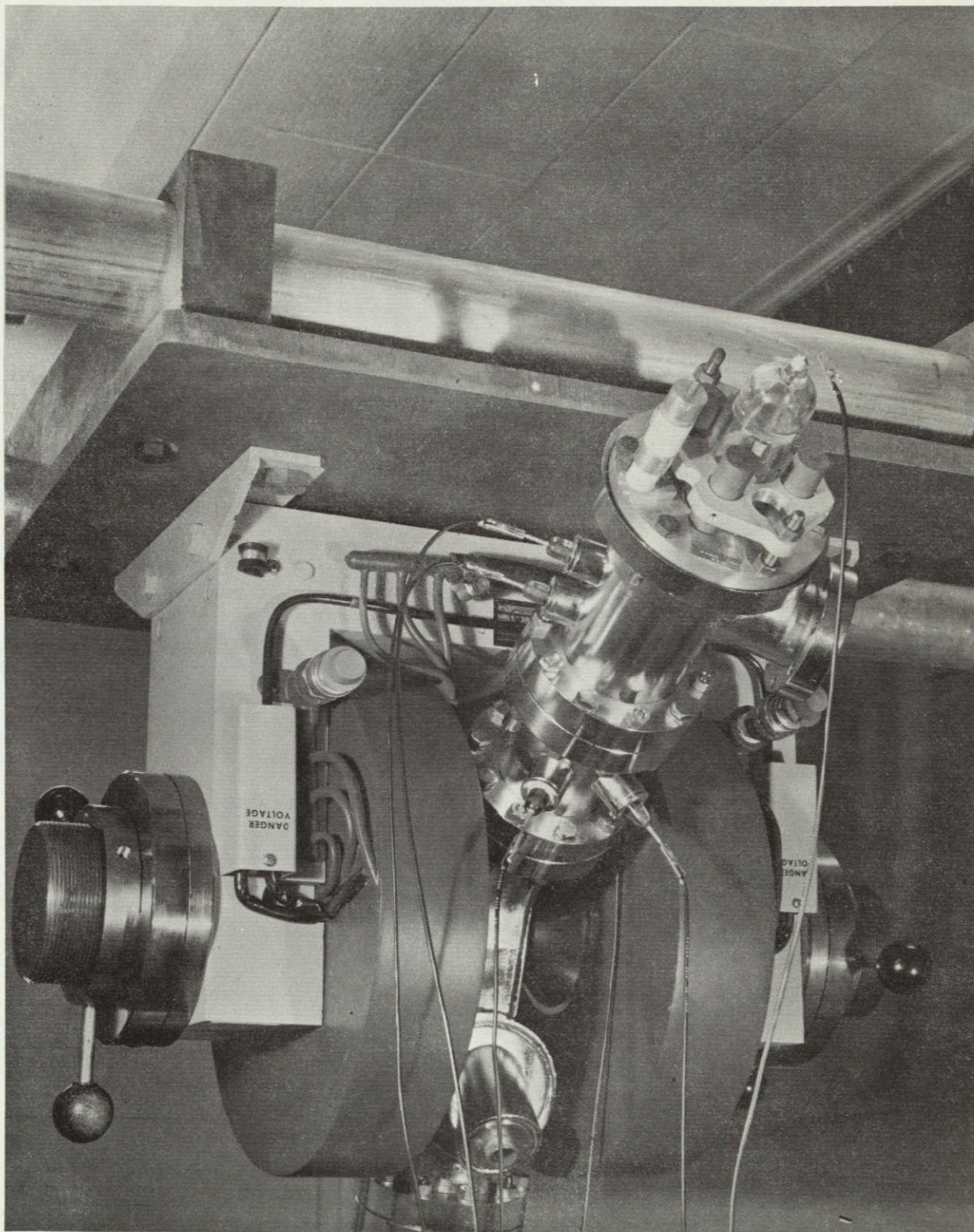


Figure 6 PROTON SOURCE, EXTRACTOR LENS AND 1st EINZEL LENS

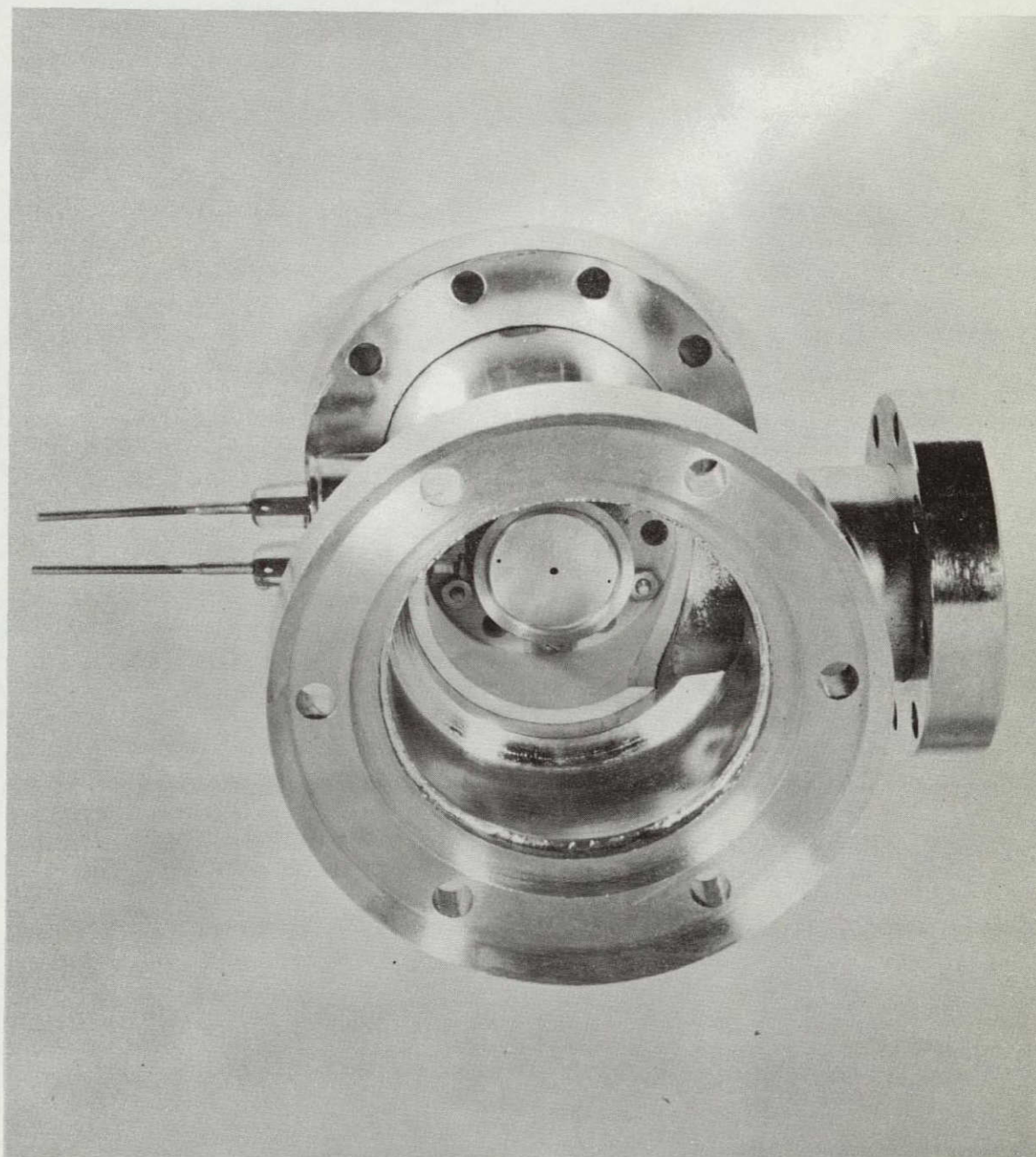


Figure 7 TWO-ELEMENT EXTRACTOR LENS (DISASSEMBLED)
TO REDUCE FLUX FROM RF SOURCE

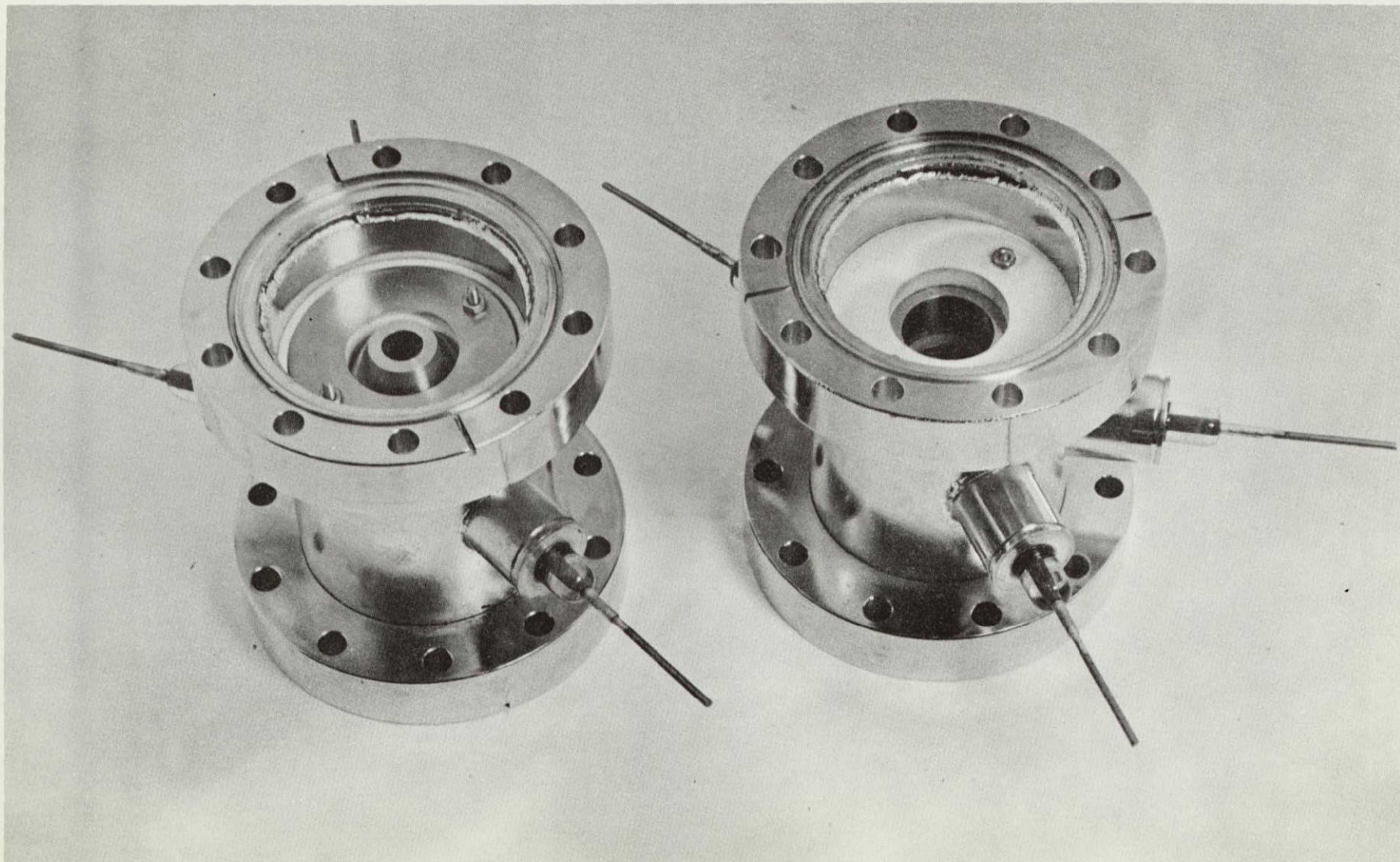


Figure 8 EINZEL LENSES; TWO VIEWS

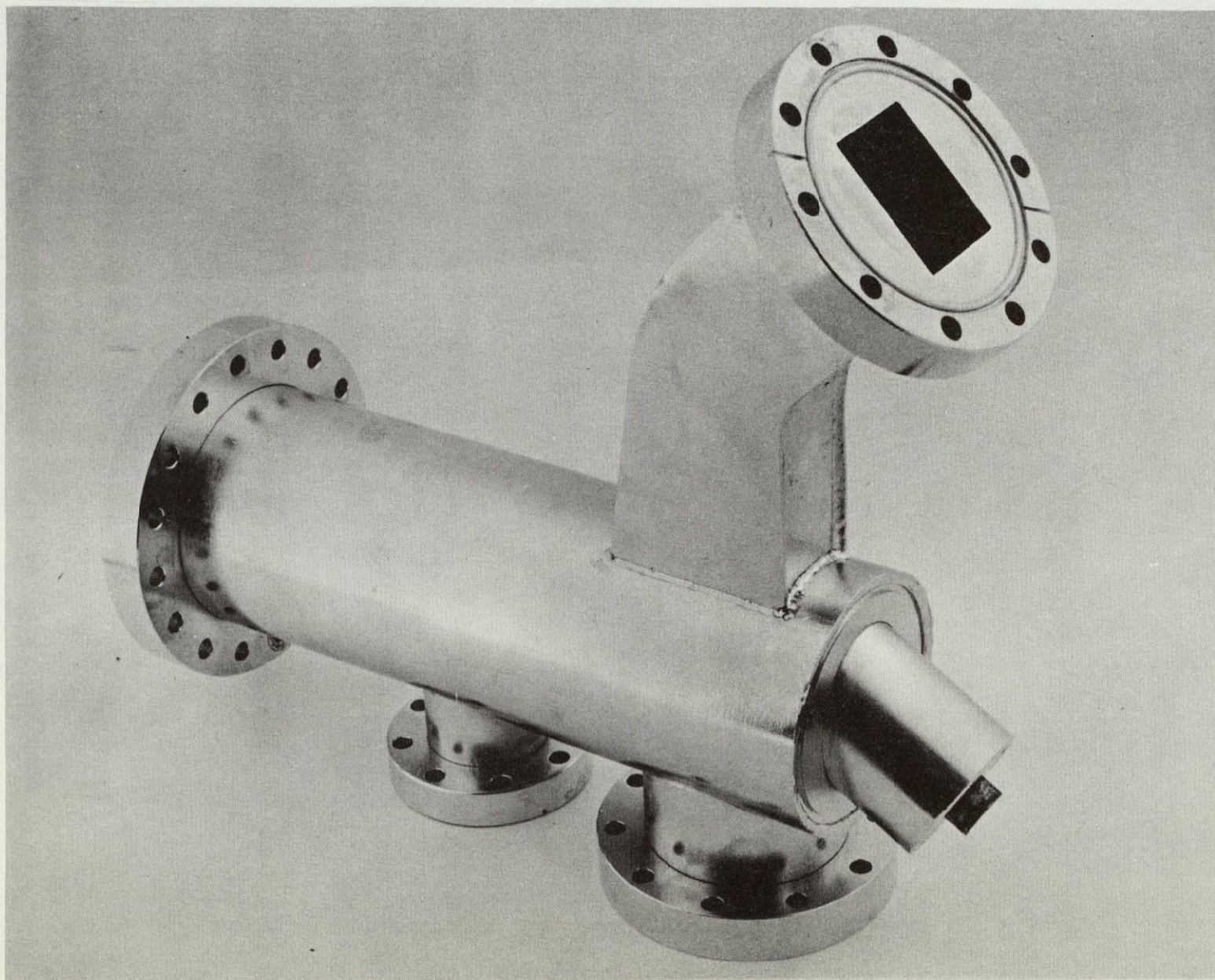


Figure 9 45° BEND (FOR MAGNET) AND FARADAY-CUP HOUSING

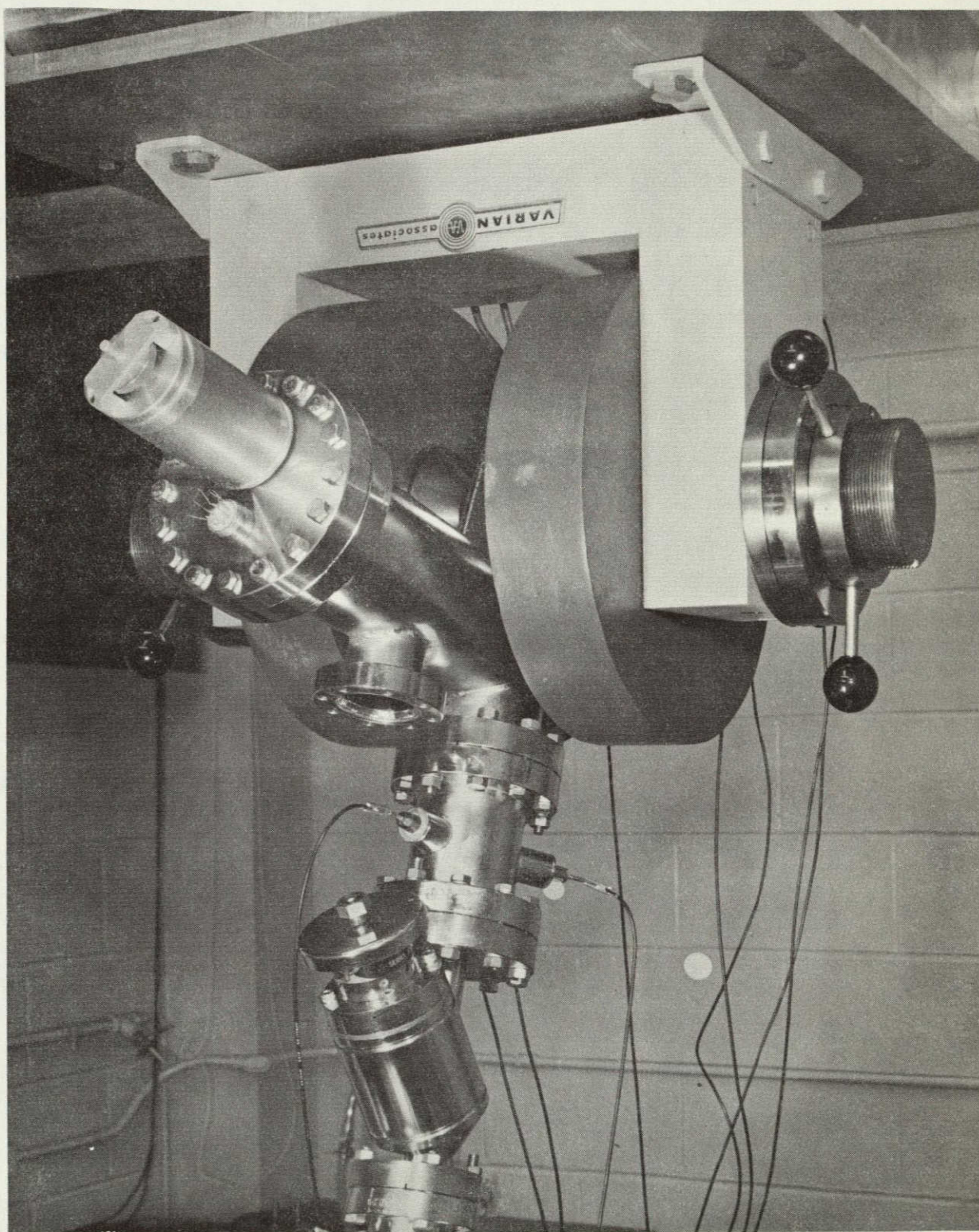


Figure 10 MASS SEPARATOR AND MASS ANALYZER
(SHOWING SECOND EINZEL LENS)

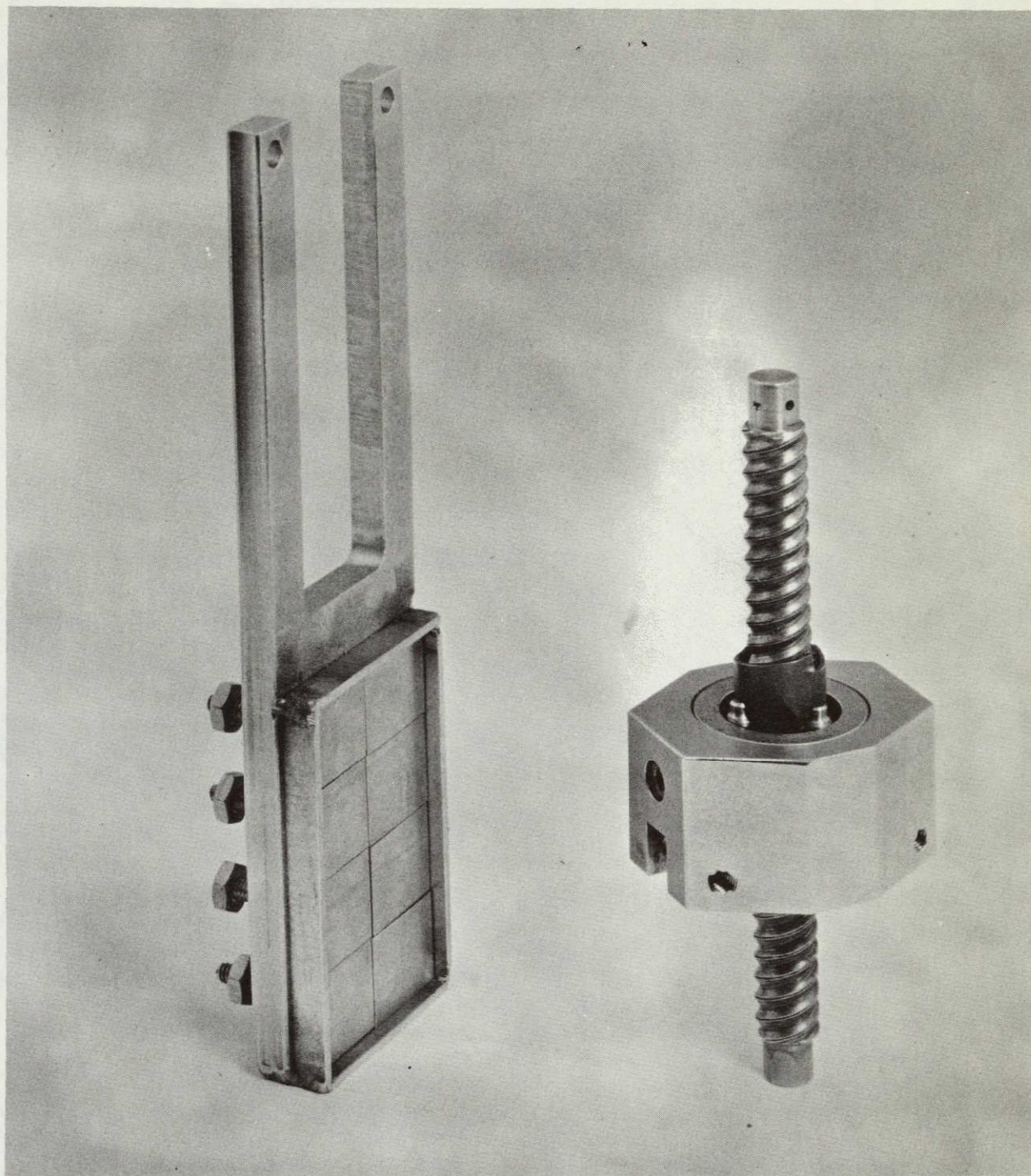


Figure 11 FARADAY CUP FLUX MAPPER

and is presented as a disassembled unit in Figure 12; this element is integral with the vacuum plate that is the basic attachment to the multiple-source adaptor housing (shown in Figure 3) for the entire accelerator assembly. (The multiple-source adaptor housing connects the proton accelerator to the basic IRIF and possesses ports for simultaneous irradiation with protons, ultraviolet light, and low-energy electrons.)

3. Charged Particle Interactions - General Theory and Remarks

Charged particles lose their kinetic energy primarily in interactions with the deeper-lying electronic levels of an atom. As a fast-moving particle approaches an atom lying in its path, part of its energy is transferred through the coulombic field interaction to the electrons of the atom, with the result that some of the electrons are either expelled (the atom is ionized) or are raised from their ground states to highly excited states; some of the atoms may be ejected also. Some of the ejected ions and electrons, in turn, possess sufficient energy to displace, ionize and excite other atoms. The probability of energy transfer is greatest for multiply-charged, slow-moving particles. The passage of charged particles through matter therefore involves a series of interactions, the nature of which depends upon the charge and initial energy of the particle. As it slows down, its potential for causing displacements and thus secondary interactions decrease; the probability for direct ionization also decreases with decreasing velocity - until finally only minor excitations will occur. The interactions most important in terms of optical stability are displacement of atoms, ionization, and excitation. By no means do all of the displaced atoms or excited electrons remain permanently away from their previous or similar equilibrium positions; most in fact, do return. One should note therefore that the excitation process is followed by a recovery (luminescence) process in which x-rays and ultraviolet radiation are emitted. It is thus highly probable that charged particle effects will include damage due to high energy electromagnetic radiation as

IIT RESEARCH INSTITUTE

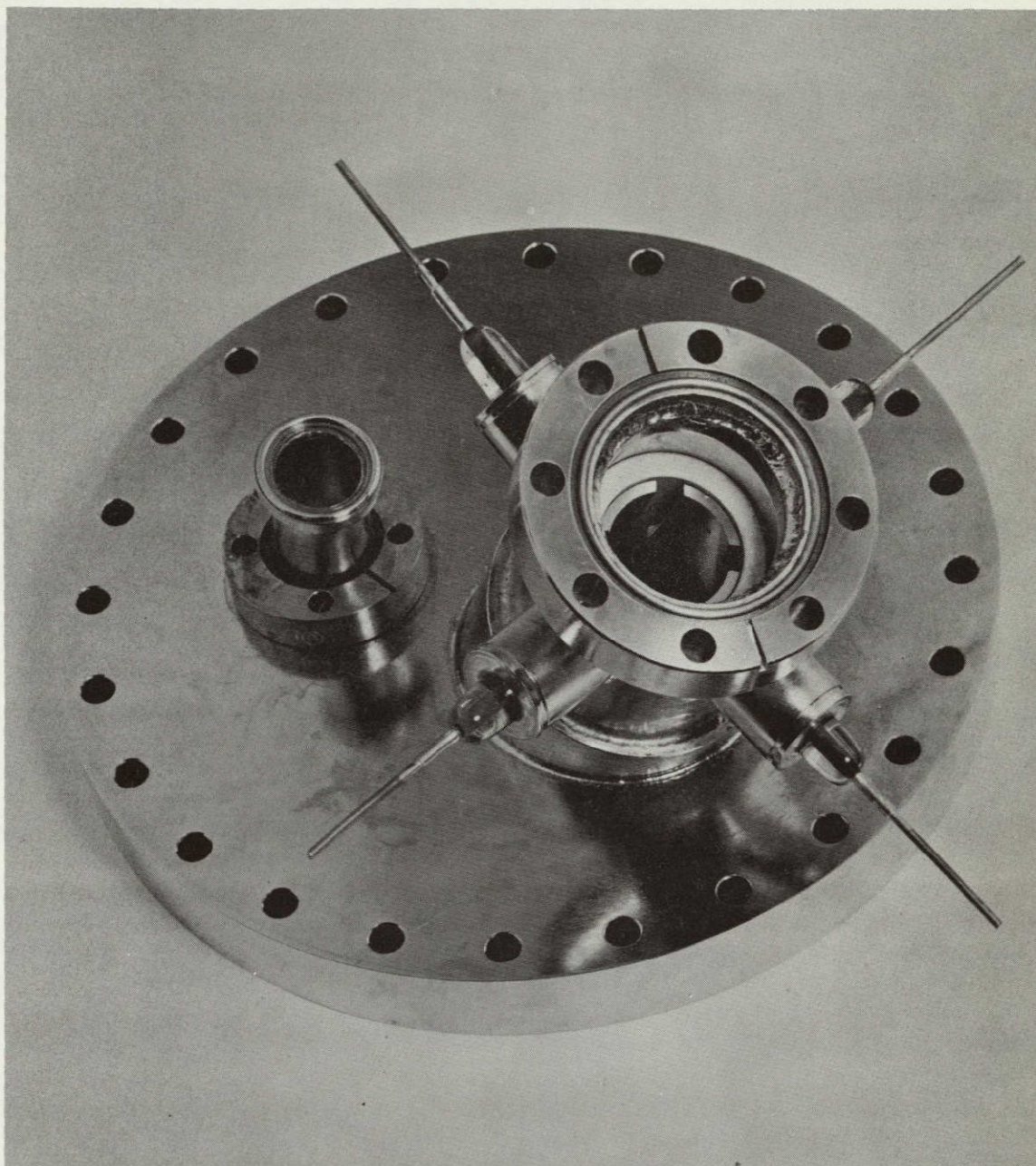


Figure 12 EJECTION LENS (SWEEP/COLLIMATOR)

well as that due to atomic displacements and chemical reactions (for example, with protons). Each incident proton will generate a multitude of hard ultraviolet photons. Longer wavelength radiation not being present, the damage is generally much less subject to radiative bleaching.

Seitz (Ref. 5) set forth the basic theory of charged particle interactions.

For energetic reactions, in which the particle velocity greatly exceeds the orbital electron velocities in the struck atom, we can use the overall energy loss rate of a particle from the expression:

$$\frac{-dE}{dx} = \frac{4\pi z^2 e^4}{M_e V_p^2} N_o Z \log(\epsilon/B) + \frac{2\pi z^2 e^4}{\epsilon} Z_i \log(\epsilon/B_i), \quad (1)$$

where

$\frac{dE}{dx}$ = the energy loss per unit distance per incident particle

z = number of charges on the charged particle

e = electronic charge

M_e = electronic mass

V_p = velocity of charged particle

N_o = density of stationary atoms

Z = atomic number of stationary atoms

B = a parameter characteristic of the electronic energy structure of the stationary atoms (of the order of the ionization potentials)

Z_i = number of electrons per atom in the outer shell, and

B_i = an energy parameter characteristic of that shell (similar to B).

The energy loss spent in displacement of atoms per incident charged particle can be calculated from

$$\frac{-dE}{dx} = \frac{2\pi z^2 Z^2 e^4 N_o}{M V_p^2} \log\left(\frac{E}{E_D} \cdot \frac{4\mu^2}{mM}\right) \quad (2)$$

where

m = mass of the charged particle, and

M = atomic mass of stationary atom.

The displacement energy, E_D , is the minimum energy which must be transferred to an atom to eject it from its lattice site.

These equations show that the rate of energy loss is directly proportional to: material density, charge on the moving particle, and the atomic number of the stationary atom; and that it is inversely proportional to: the energy of the moving particle, and, in the case of displacements, to the mass of the stationary atom, and the displacement energy. The rate of displacement can be calculated from Eq. 2 and from knowledge of the rate of charged particle incidence and the displacement energy. This gives a rough idea of the instantaneous rate of formation of interstitials and vacancies (potential color centers).

Regarding the fates of displaced ions and electrons, it is a fortunate fact that the actual induced vacancy and interstitial concentrations of irradiated materials are orders of magnitude less than those calculated from theory; this is because the displaced atoms/ions eventually return to the vacancies they generated. The estimation of induced vacancy and interstitial concentrations therefore bears little relation to the actual permanent concentrations of these defects. In summary then, charged particle damage is certain to produce effects which ultraviolet produces, as well as some which result from massive interactions, and in combined radiation environments radiative bleaching is undoubtedly going to create "synergism" and invalidate any reciprocity which might have existed in single environment testing.

B. Space Simulation Criteria - A Discussion

1. Real Versus Simulated Space Environments

Ideal simulation implies exact duplication of the real space environment, not simply the effects of the real space environment. Since the nature and composition of the real space

IIT RESEARCH INSTITUTE

environment differ from one place to another; the effects likewise differ. For example, the environment at 500 miles above the earth's surface differs very much from that at an elevation of 20,000 miles. However, beyond the radiation environment trapped in the earth's magnetic field, the space environment becomes uniform or fairly uniform and depends only upon distance from the sun. That environment in which the solar wind is active, the deep-space environment outside the earth's magnetosphere, consists primarily of solar electromagnetic and particulate radiations. To duplicate these in a laboratory we must have a reasonably good characterization of the solar electromagnetic spectrum as well as the solar particulate radiations; the former is well known, the latter is reasonably well known (Ref.'s 6, 7). There are, however, several other important questions involved in designing and operating simulation equipment and in the evaluation of the data.

First, and foremost, it is essential that in an operating system the response of materials be as nearly as possible the same as their response would be in the actual space environment. This condition is met when the exact conditions of the space environment are duplicated, i.e., when the electromagnetic spectrum, the charged particle energy spectrum, the rates at which both of these are incident on a surface, and when electric neutrality and prescribed vacuum-thermal conditions are achieved--all simultaneously!

A critical question is that of determining the effects of non-simulation. One has the choice of either trying to produce a system which precisely simulates the space environment or of accepting a system which will produce in real materials a response identical to that which the space environment would induce. These are ideal choices, however, and it is one of our objectives to see how closely the first choice, exact environment simulation, can be realized.

There are three factors in this question: the spectral energy distribution of the components, their relative compositions and

their flux rates. In a laboratory situation all these have to be simulated in order that the effects on the material will be realistic. As a matter of practicality the effects of nonsimulation with respect to composition must be determined, for example, for a beam with 50% H^+ versus one with 95% H^+ (ionized hydrogen). Rates of irradiation also might be important, particularly if the rates of the various ionized species are different than their respective rates in the space environment. In multiple environment simulation tests the complexity becomes extremely great.

In practice we do not achieve exact environment simulation; hence we must determine which parameters are most important in terms of simulation. The effect of a major parameter, if different from what it should be, may be quite serious. Consequently, the important parameters must be correlated quantitatively with their effects.

Guidelines for designing and operating simulation equipment are a necessity, not only to assess the effects that each component has on defining the character of the proton beam but also to understand the interactions of components and the system performance as a whole. For example, while it is important to know the extent of energy broadening occurring in an acceleration lens, it would also be important to know how differently the next and other successive lens would have to be operated to compensate for it (and it would be very important to know the response of materials as a function of the energy spread).

2. The Charge Build-Up Problem

The incidence of protons upon a dielectric material will always create a charge build-up in the material. This is true because the reaction of the proton (or positive ions in general) with the dielectric material implies the accumulation of a positive charge. This positive charge is further compounded by a secondary electron release in the case of energetic ions. In most materials the rate at which these secondary electrons are emitted can and often is higher than is the rate of incidence of

the charged particles producing them. The net charge buildup therefore proceeds at a rate higher than that due to the proton beam alone. Whether or not these conditions exist in space is a question of major significance. In our opinion, it is not possible for a very large voltage to build up on a spacecraft coating simply because the solar wind is electrically neutral (Ref. 8). The build up of a positive charge would in fact attract more strongly the electrons and tend to repel protons. This buildup also would tend to attract the secondary electrons back to the surface so that the net charge buildup could not possibly get much beyond the material's work function (for the escape of electrons). This is of the order of possibly 5 to 10 electron volts. In the CREF the secondary electrons which escape from the samples are replaced by a thermal ion source. Although it can be argued that there is some buildup of charge due to an excess positive charge on the coatings it is hardly likely that this buildup can be significant enough to effect spectral reflectance. In our opinion, however, this question is not completely resolved. Yet it is our belief that charge build-up is not a significant problem on a space vehicle. It should, therefore, not be permitted in simulation facilities.

3. Simulation Parameters

The important parameters in solar simulation and in solar wind simulation are the spectral energy distribution of the protons, of the solar electromagnetic radiation and the vacuum level. The vacuum level is important in the sense that the vacuum system must be such that the net pressure effect of space is simulated, that is, that a molecule leaving a surface will not return to it.

Achieving the correct energy distribution and average energy level of the protons in the solar wind is a difficult task. In practice, the methods for doing this are generally divided into two categories -- one is electrostatic, the other magnetic. Separation is a parameter that determines the amount of H_2^+ , H_3^+

and other species that may be incident upon the samples. The term separation generally refers to the geometrical relationships between the components of an analyzed beam. Since the magnetic separation is energy-selective, there will be an energy separation as well. Thus, for a given magnetic field the protons with the highest energy (in a Maxwellian distribution) will not be bent as much as the lower-energy protons, while the lowest-energy H_2^+ ions will be bent most, and there may be a geometrical overlap. This is illustrated in Figure 13, where it can be seen that the beam incident on the x-axis after separation have an energy distribution along the beam-isolation plate. In space the separation parameter for H^+ is of the order of .96, i.e., the ratio of H^+ to everything else. The solar wind, therefore, is effectively simulated by a pure H^+ beam along with the accompanying thermal electrons which provide an essentially neutral beam. In practice there also has to be a uniformity of the incident beam. Consequently, uniformity becomes a practical requirement. The rates at which the particles strike the surface along with the rates of the solar electromagnetic radiation should be very nearly that of space. The ratio of the two fluxes (particulate and electromagnetic) should be very nearly unity; that is, the ratios of the intensities of these two fluxes should be very nearly that of the space environment.

The solar wind consists of 2.5×10^8 protons/cm²-sec with ion energies centered approximately at 1.8 keV; they may rise during solar flares to approximately 5 keV, where the energy distribution of these protons is of the order of 0.01 of the maximum energies, or .01 of the average energy (in other words about a 1% spread of energy). In practice the flux rate corresponds to a current level of 4.0×10^{-11} amp/cm². The methods that are used to determine the degree to which a simulation device is achieving its purpose are difficult to decide upon. The detector/monitor for a solar wind simulator must be a Faraday Cup which has the capability of scanning the entire beam to

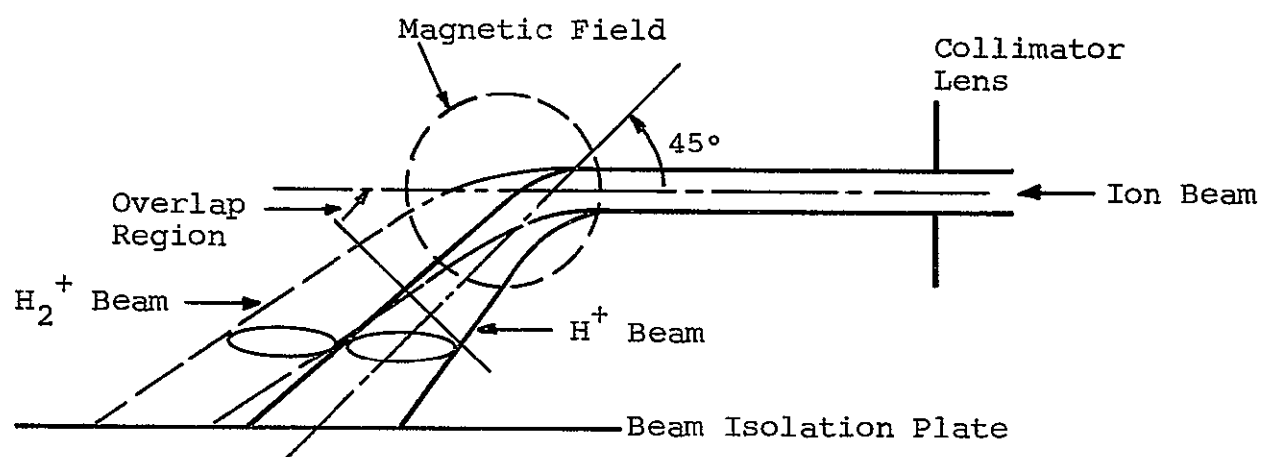


Figure 13 MAGNETIC ANALYSIS AND PHYSICAL ISOLATION OF PROTON BEAM

measure its intensity in a horizontal plane. It must also be able to measure the intensity of the beam on a unit area basis and it must be able to scan the beam energy distribution. Consequently, devices for measuring both the flux incident per unit area and the energy of the beam itself must be provided at the sample location. The total environment of the samples must be such that they will respond to the incident beam solar electromagnetic and particulate radiations in very much, if not identically, the same way they would respond in space. Consequently one must also provide a charge buildup detector, because in reality the buildup of charge induced by proton reactions will occur and provisions for effectively neutralizing the charge must be provided.

C. Performance

1. Objectives

The calibration and characterization measurements performed on the CREF have been quite successful. The system has been under test for approximately 6 months and is now operational. In general, the CREF operates quite well within the tolerance levels that were anticipated. Major operational problems have not occurred. Numerous minor ones have kept the system from being operational at an earlier date. However, our experience with the CREF indicates that the basic design of the system as a whole is fundamentally sound. Individually, the components and ancillary equipment operate well within satisfactory limits. Typical of some of the minor problems that we have encountered to date was the necessity for maintaining the system electromagnetically shielded (i.e., not allowing RF to get out of the building). Numerous electrical problems have occurred; ground connections and ground loops, interaction between instruments and power grounds, faulty connectors and connections, etc. have kept appearing. Components also have often given us problems because of poor construction, insufficient ratings, or general defects. Operational problems have been relatively minor except

for a number of vacuum leaks, ion-pump failures and secondary electron emission. The inability of operators to recognize or detect certain performance flaws has been removed with experience.

The system is sufficiently complex and the diagnostics of its performance are so complicated that in most cases it is very difficult to interpret the experimental results or correlate them from one test to another without making a great effort to ensure that all the important operating conditions are well known and under close control.

The objectives of these activities were mainly to determine the effects of each of the major parameters on the performance characteristics of the system as a whole. In general, we have wished to vary the proton flux at the sample locations from roughly one solar wind, or 4×10^8 protons/cm²-sec, up to approximately 25 solar winds, or 10^{10} protons/cm²-sec. We have also wanted the beam purity, that is the proton (H^+) species, to be greater than 95%, and approximately $\pm 5\%$ energy spread about the effective energy. Geometric uniformity at the sample location is a little more difficult to achieve in most cases; for example, the microscopic flux at the sample location should be within 20% of the total beam flux averaged over the whole sample location.

These objectives have largely been met and the effects that each of the major components have on these individual performance objectives have been determined.

2. Characteristics of Operation

Rather than indicate the effects each component (for example, each Einzel lens) may have on the succeeding elements and eventually on the conditions at the sample position, we will present some of the more important variables which fix these conditions or have the most important effect on them.

The probe voltage, which is a positive voltage applied directly to the RF-source tube, determines directly the beam energy. This voltage is critical; the voltage drop between the

power supply and the probe must be accounted for or made extremely minimal. The actual energy of the protons emanating from the system is slightly less by some small amount (roughly 25-30 eV) than the actual set energy as determined by the probe voltage. The probe voltage also affects the flux and the ionic composition of the emergent particle flux. All of these, of course, affect the strength of the magnetic field required to separate (analyze) the protons, and this in turn affects the focal properties of the beam, the space charge, and the energy distribution of the beam.

We have found in measuring, or monitoring, the proton flux that it is very important to account for the secondary electron emission. The net effect of the secondary electrons is to increase the apparent beam flux so that the actual beam flux is slightly less (sometimes much less) than the apparent flux. At approximately 1.2 kilovolts (kv) the correction is of the order of 20%. At 2 kv the correction is of the order of about 2% (for aluminum targets). In other words, an indicated flux of 2×10^8 2-keV protons would in fact be 1×10^8 under these conditions.

To measure beam purity, the separated (individual) beams are scanned across the Faraday Cup using the magnetic separator (or analyzer) and the resulting scan of Faraday Cup current (beam intensity) versus magnetic field strength (such as Figure 14 shows) can be used to determine the magnetic separation between the two beams and the amount of field strength required to produce these two beams at their individual locations on the Faraday Cup. Since the Faraday Cup is divided into eight elements (see Figure 11) each of known size and geometrical relationship to one another, the beam can be tracked across each of the cups and the amount of field strength required to move it from one element to another can then be determined. The purity then can be determined by the fact that, sufficiently far from the magnet, the divergence of the two beams, H^+ and H_2^+ , is great enough to cause them (these respective beams) to hit different elements of the Faraday Cup. This divergence ordinarily is greater than the diameter of the

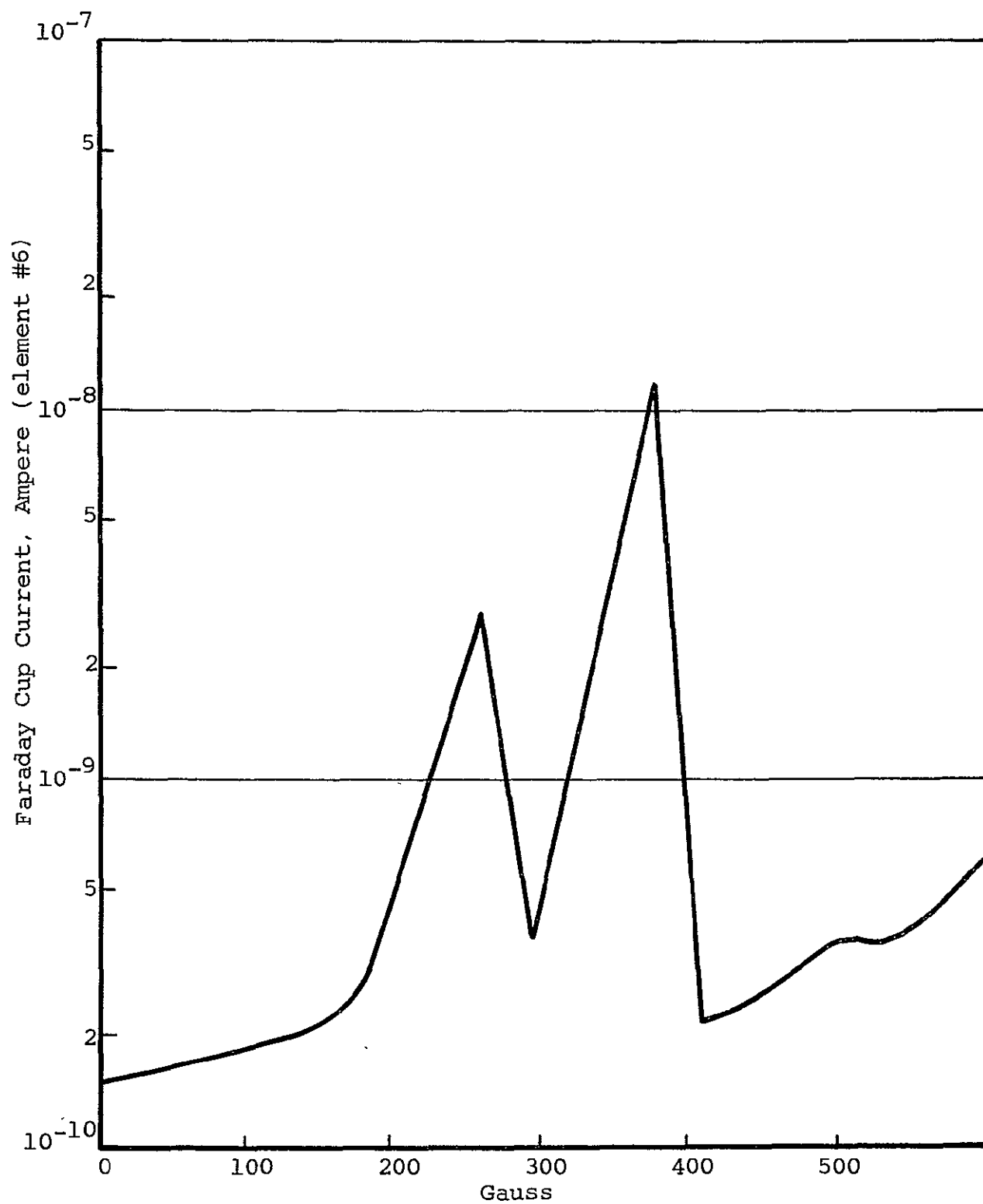


Figure 14 ION CURRENT VS MAGNETIC FIELD STRENGTH, GAUSS (B-SCAN)

downstream aperture into which one beam or the other is effectively focused. In effect the H^+ beam (first peak) is focused directly into the downstream aperture and only that part of it is focused which is at the top of the peak. Beam purity is thus achieved by magnetic separation followed by geometric isolation. The beam energy spread is determined by a scan, such as presented in Figure 14, in which the bias potential on the Faraday Cup is increased up to the order of the beam energy. When the current drops effectively to zero, the shape of the curve in this region is related to the energy spread (indicated by the dotted line). The peak of the distribution is at the effective energy of the proton beam. The width of the curve indicates its energy spread and this is taken to be the energy difference between the half power points as indicated by the $\pm E_{1/2}$ points on the curve. For an energy of 1.2 kv this energy spread has generally been of the order of about 50 volts; the total spread has been slightly less than about 1/10 of a kv or less than about $\pm 5\%$. Beam uniformity has been measured at the sample location using a 23-element Faraday Cup detector (shown in Figure 15). In this method the entire Faraday Cup is placed above the sample location and all 23 locations, or elements, of the Faraday Cup are scanned. In general, the quadrupole lens has a fairly strong effect on the beam uniformity. The beam can be spread out across all of the samples by simply increasing the voltage across any two of the lenses. A voltage of approximately -800v applied on two of the four quadrupoles gives a beam uniformity of about 80%. Each element of the detector is one cm^2 in cross-section and the geometric relationship between each detector is known; hence the relative flux uniformity throughout the sample area can be determined quite well. Intensities at the center of the sample location were determined to be of the order of 1.1×10^{-10} ampere/ cm^2 which is roughly 4 solar winds. Correcting for secondary-electron emission, this flux would be slightly less than 4 solar winds.

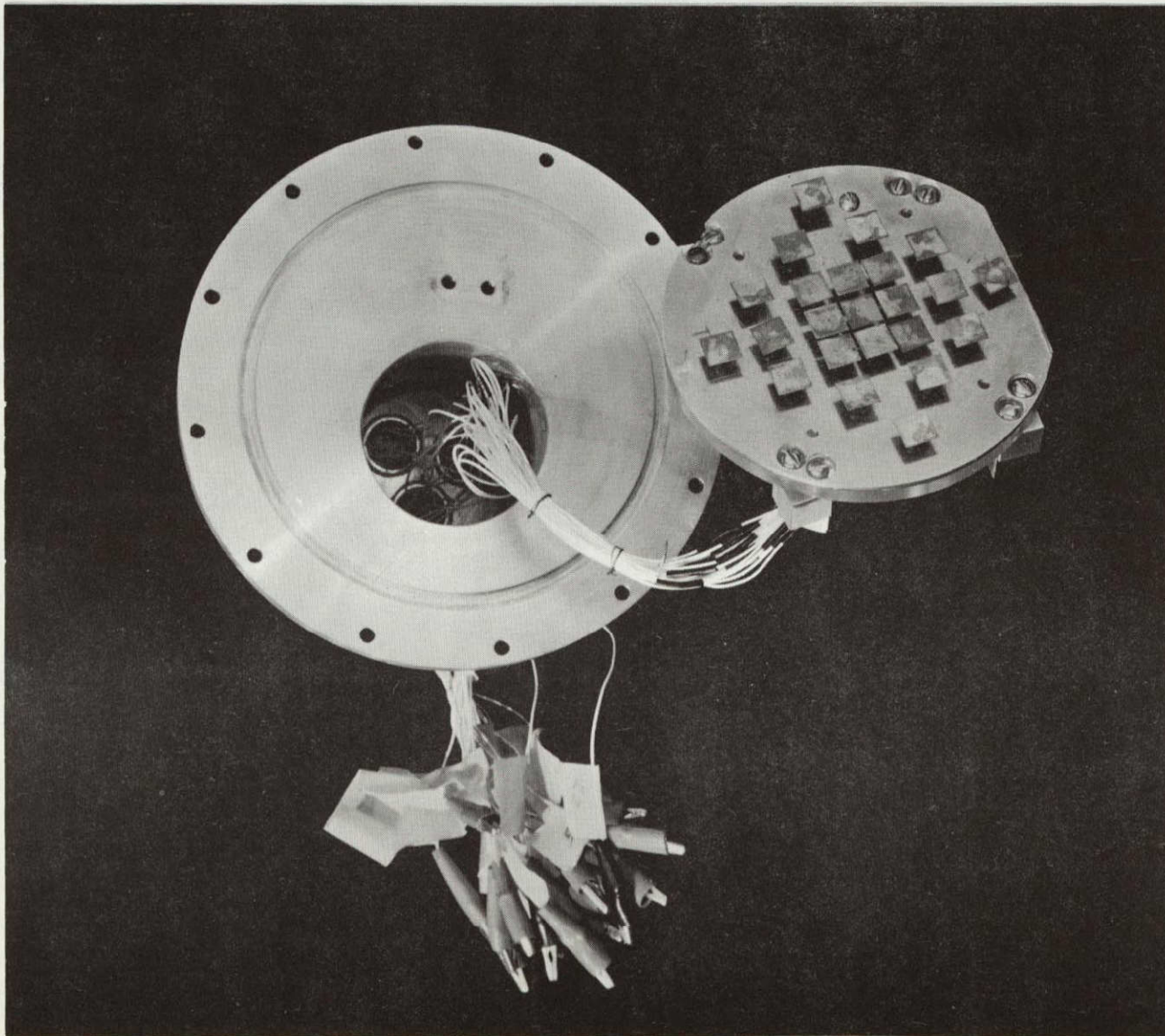


Figure 15 23-ELEMENT FARADAY CUP FOR BEAM MAPPING AT SAMPLE LOCATION

The total flux or the flux at the sample location can be decreased to a flux of the order of 1 solar wind by one of several means. An aperture located just above the second einzel lens can be installed with a much smaller diameter; another possibility is increasing the voltage potential on the first collimator lens.

Figure 16 shows the relationship between the potential applied to this lens and the resulting maximum flux at the sample location; on the right side of the figure are the intensities in solar winds. Figure 17 shows the flux distribution over the sample area at the sample location. This plot is at full scale and shows the beam energy distribution, the samples and the Faraday Cup elements superimposed upon each other. Figure 18 is a plot of the total flux at the sample location versus the voltage required to suppress it.

3. Operating Conditions

We have found a number of operational procedures which seem to stabilize and regulate the beam intensity. The hydrogen supply system was found to be quite critical. We use a very high-purity (research-grade) hydrogen gas. We pass this through a regulator and control the inlet pressure to a palladium leak at 16 psig. The differential pressure across the palladium leak is therefore kept very constant. The intensity of the flux is maintained constant for the reason that there are no pressure surges or transients in the ion source. The heater current to the palladium leak is another critical factor. This must be highly regulated and for this purpose we use a titanium sublimation pump power supply.

The general philosophy in the development of procedures was to proceed from the ion source down to the sample location, characterizing the effect at the sample location of each of the lenses in the system. The total ion current extracted from the source is shown in Figure 19 as a function of applied (probe) potential. The relationship is essentially linear. The primary

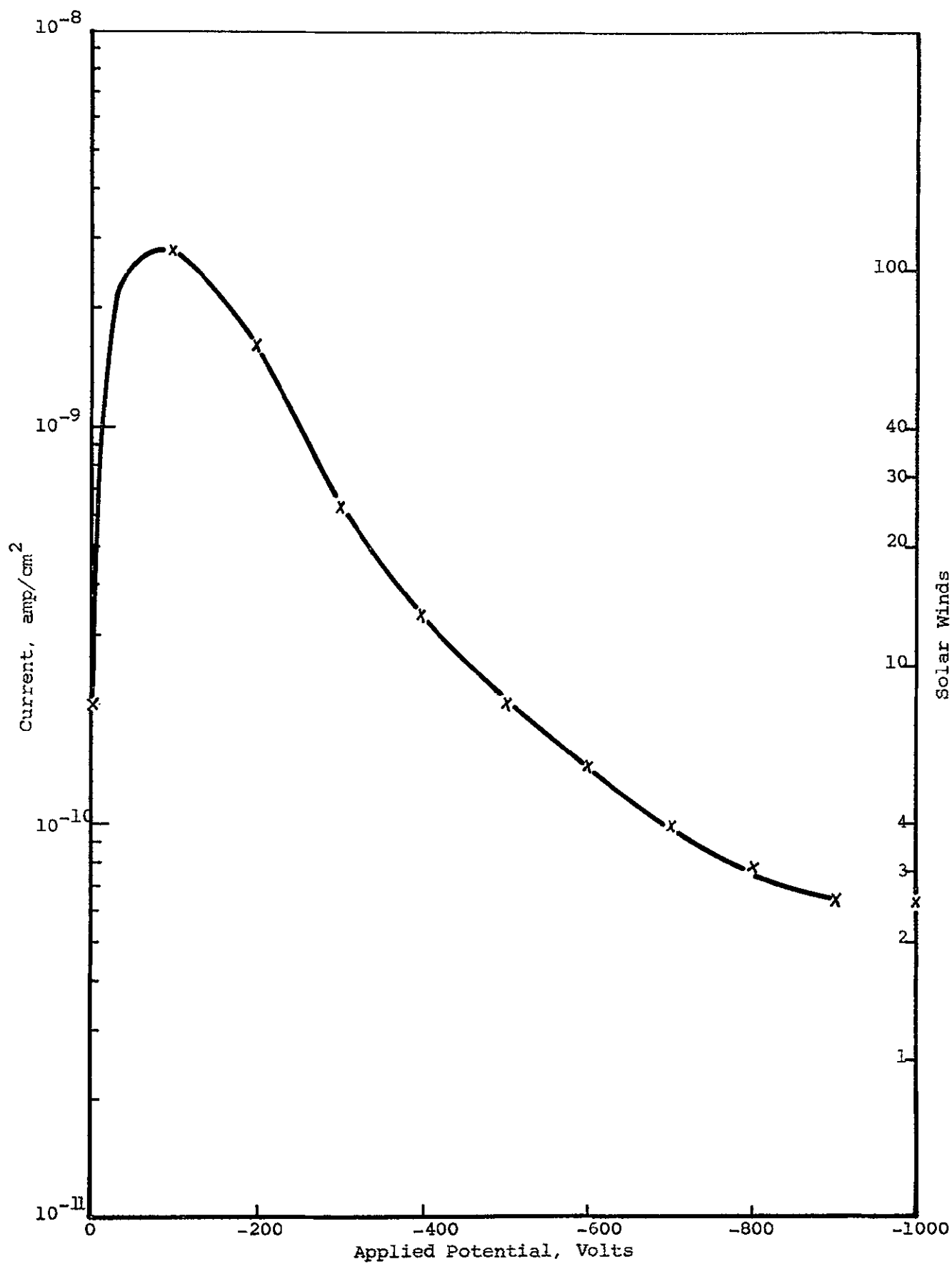
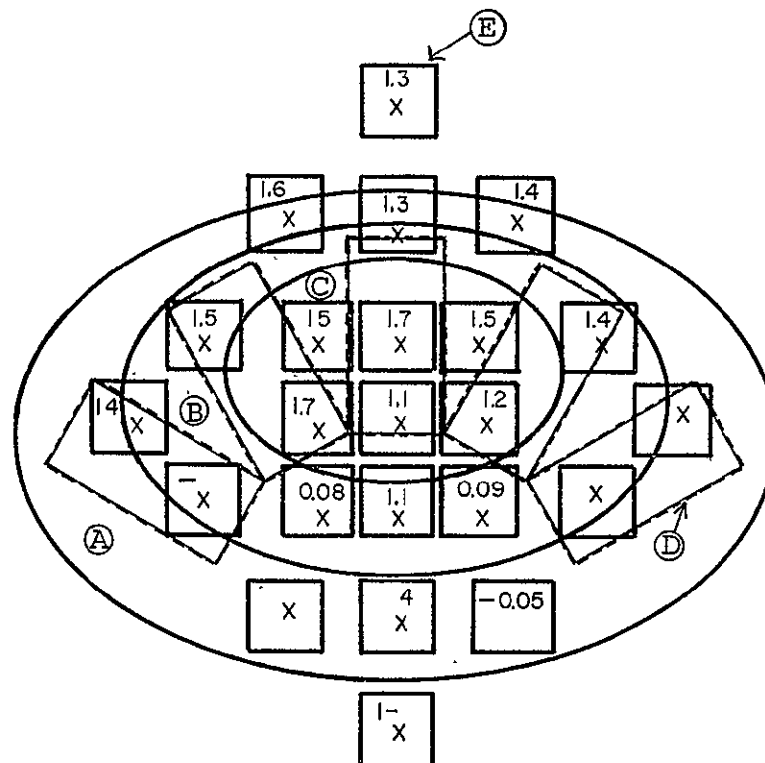


Figure 16 FLUX INTENSITY AT SAMPLE LOCATION VS COLLIMATOR LENS POTENTIAL



- Ⓐ 2 ± 0.1 SW Intensities
- Ⓑ 4 ± 0.3 SW Intensities
- Ⓒ 5 ± 0.5 SW Intensities
- Ⓓ IRIF Samples
- Ⓔ Faraday Cup (23 elements)

Note: Intensity units are in Solar Winds. One Solar Wind $\approx 2.5 \times 10^8$ p/cm²-sec.

Figure 17 FLUX INTENSITY MAP AT SAMPLE LOCATION (SCALE 1:1)

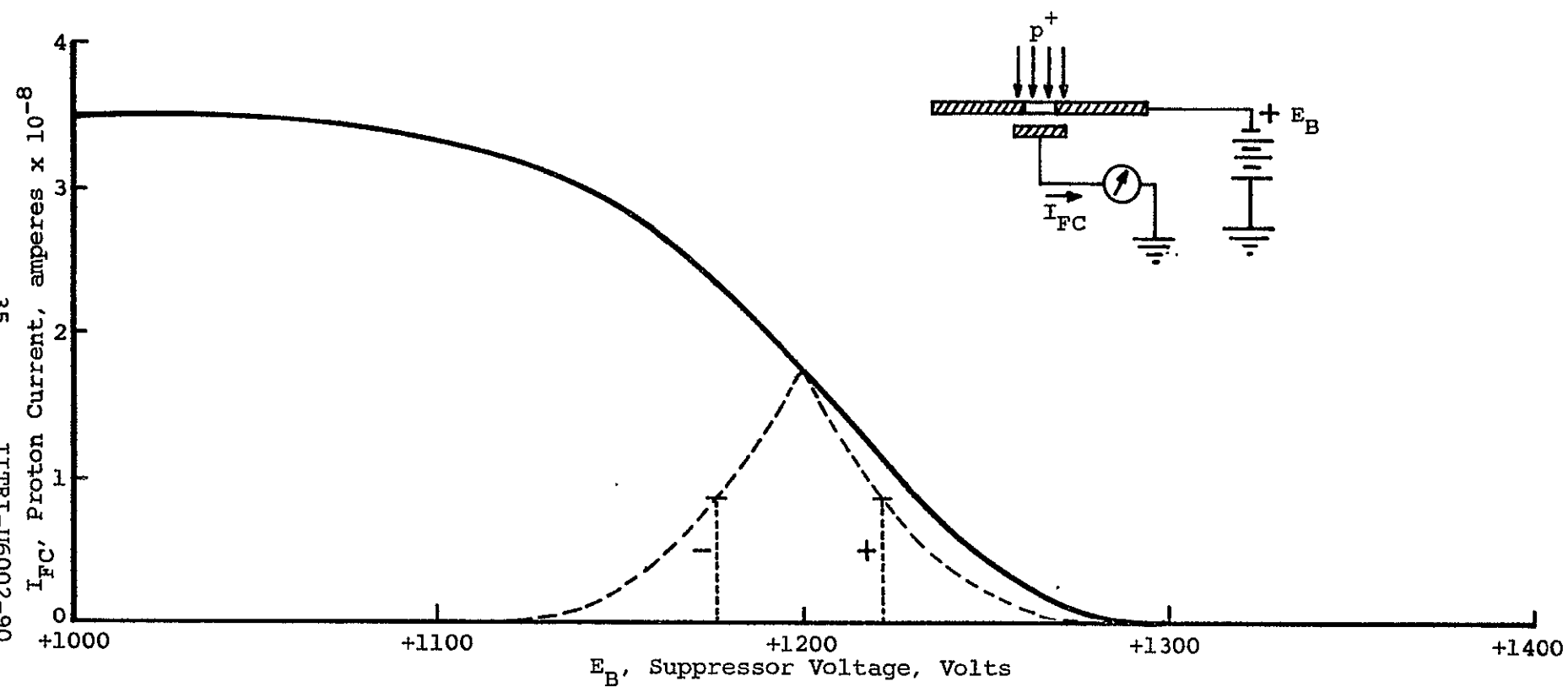


Figure 18 PROTON CURRENT VS SUPPRESSOR VOLTAGE

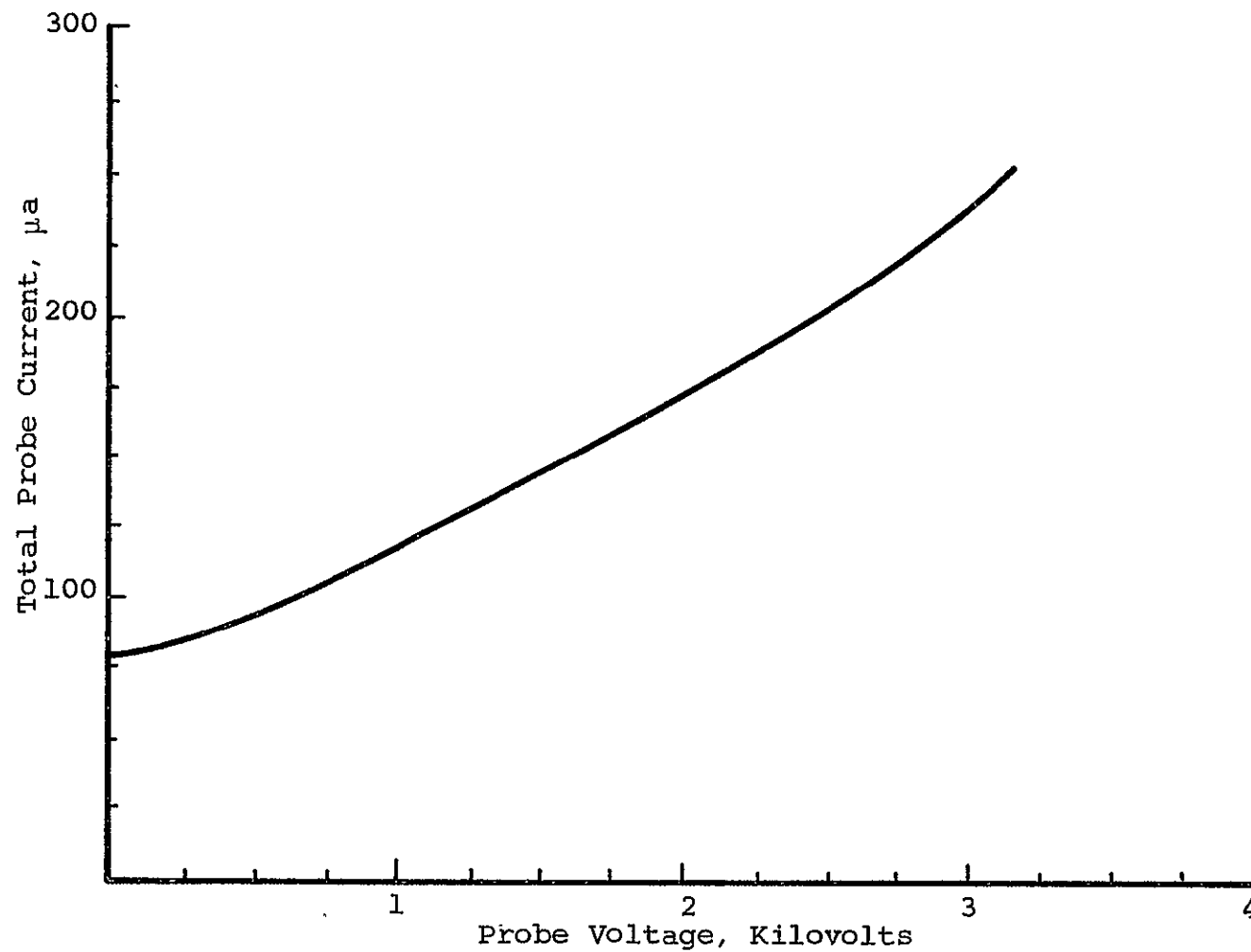


Figure 19 PLASMA CURRENT VS APPLIED POTENTIAL

investigation, however, was to determine the focusing properties of each of the lenses and the effects that each lens would have on the succeeding lens, and also, for example, the ability of the einzel lens to focus the beam into the analyzer magnet. The conditions best suited for this latter situation were found to be with the middle element of the einzel lens at approximately +800 volts, or roughly 2/3 of the probe potential, and the two outer lenses grounded. Further down the system the einzel immediately following the analyzer lens has a very small aperture which geometrically selects the H^+ beam. This lens has in all cases been grounded because the aperture on the exit side of the einzel lens was inadvertently made too small to allow the einzel lens to function effectively as a focusing element. Fortunately, however, the four quadrapole lenses have a very strong focusing effect.

The current operating conditions are: the first collimator lens is set at -1200 volts, the second collimator lens at -1300 volts, the three elements of the first einzel lens at 0, +800, and 0 volts respectively, all elements of the second einzel at 0 (ground), two of the four quadrapole elements at -830 volts and two at 0, and with zero bias on the samples.

III. RESULTS OF PROTON (SOLAR-WIND) IRRADIATION

A. Test Conditions

The results of two solar-wind simulation tests are presented. The figures shown (Figure 20 through 25) represent the form in which the in situ hemispherical reflectance data are displayed. The data, taken with a Beckman DK-1 strip recorder, is typical of the data taken with the basic IRIF-II ultraviolet facility.

The irradiations were performed at a pressure of 1×10^{-6} torr and at a specimen temperature of 12°C . Reflectance measurements were performed initially at $\sim 10^{-7}$ torr pressure and after depositing the total fluence of protons (indicated in Table 1). Three specimens were irradiated in each test (Figures 20, 22 and 25 in one test and Figures 21, 23 and 24 in the other). The voltages, conditions and the beam pattern employed in these irradiation tests were those specified in the last section (II.C).

B. Results

The effects of irradiation with $\sim 2 \times 10^{15}$ protons/cm² on zinc oxide and the two specification paints based on zinc oxide, Z93 and S-13G, are shown in Figures 20, 21 and 22. The data are summarized in Table 1. Examinations of the damage spectra show that the SP500 zinc oxide powder underwent damage in both the visible and infrared spectrum: The Z93 specimen sustained similar, but slightly diminished, damage in these two regions. Surprisingly, the S-13G exhibited only slight damage in the visible spectrum; damage in the infrared was only slightly less than for the Z93 specimen.

The effects of proton irradiation on zinc orthotitanate and zinc orthotitanate paints are presented in Figures 23, 24 and 25. Again, the pigment powder (in this case plasma-calcined Zn_2TiO_4), Figure 23, exhibited the greatest damage in the visible spectrum, while the silicone paint (in this case, based on Owens-Illinois 650 resin) exhibited no visible-region damage. The acid phosphate-treated pigment prepared as a potassium silicate paint (Figure 24)

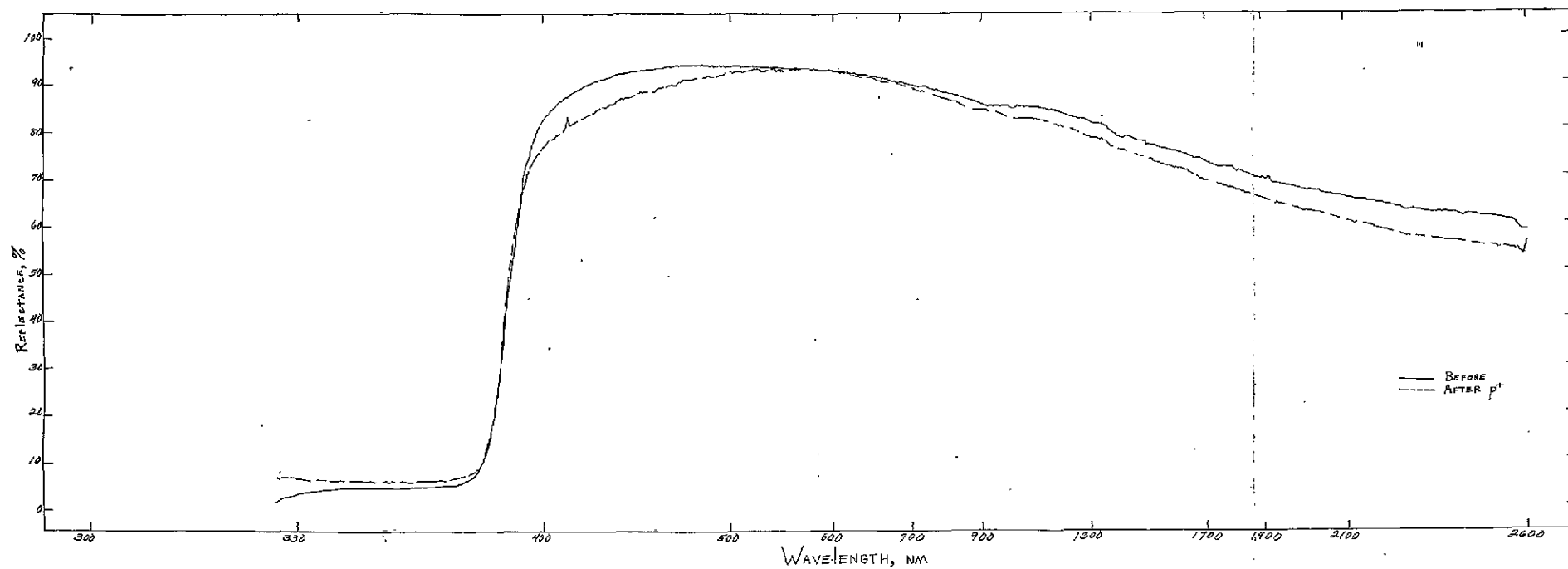
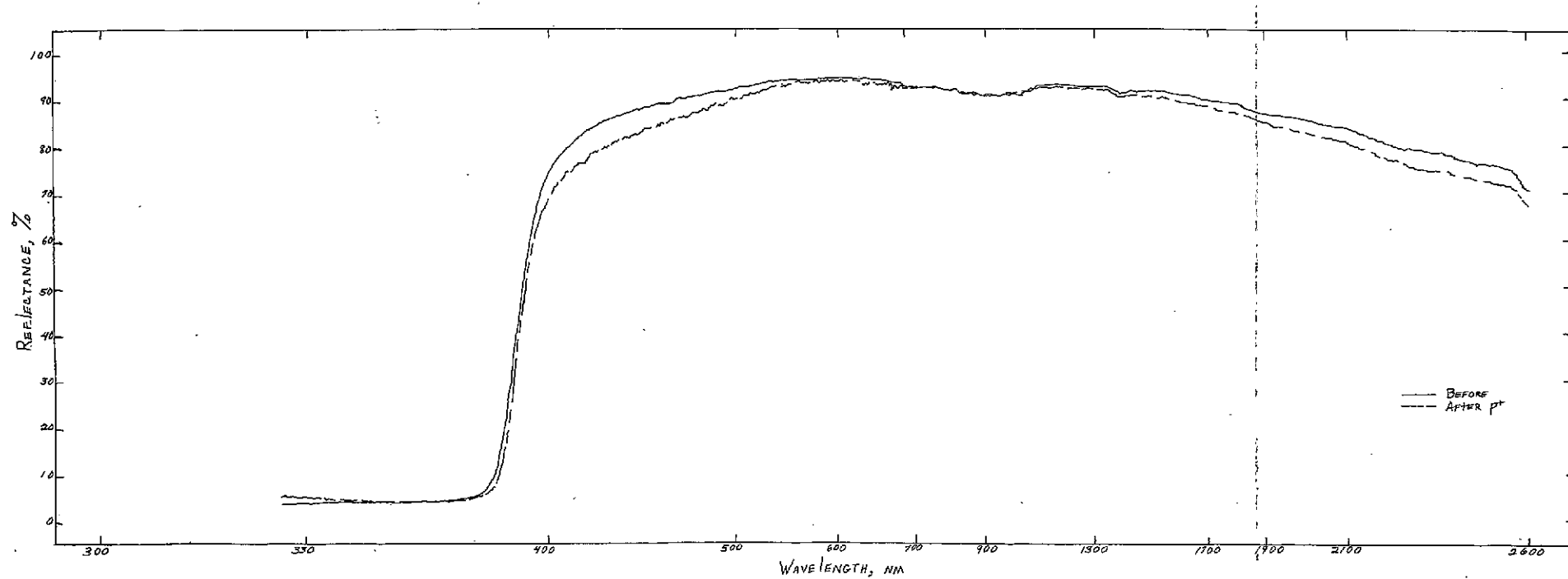


Figure 20 EFFECT OF 2.5×10^{15} PROTONS/CM² ON IN SITU
REFLECTANCE SPECTRA OF SP500 ZINC OXIDE



1

Figure 21 EFFECT OF 2.7×10^{15} PROTONS/CM² ON IN SITU REFLECTANCE SPECTRA OF Z93 THERMAL-CONTROL PAINT

FOLDOUT FRAME 1

FOLDOUT FRAME 2

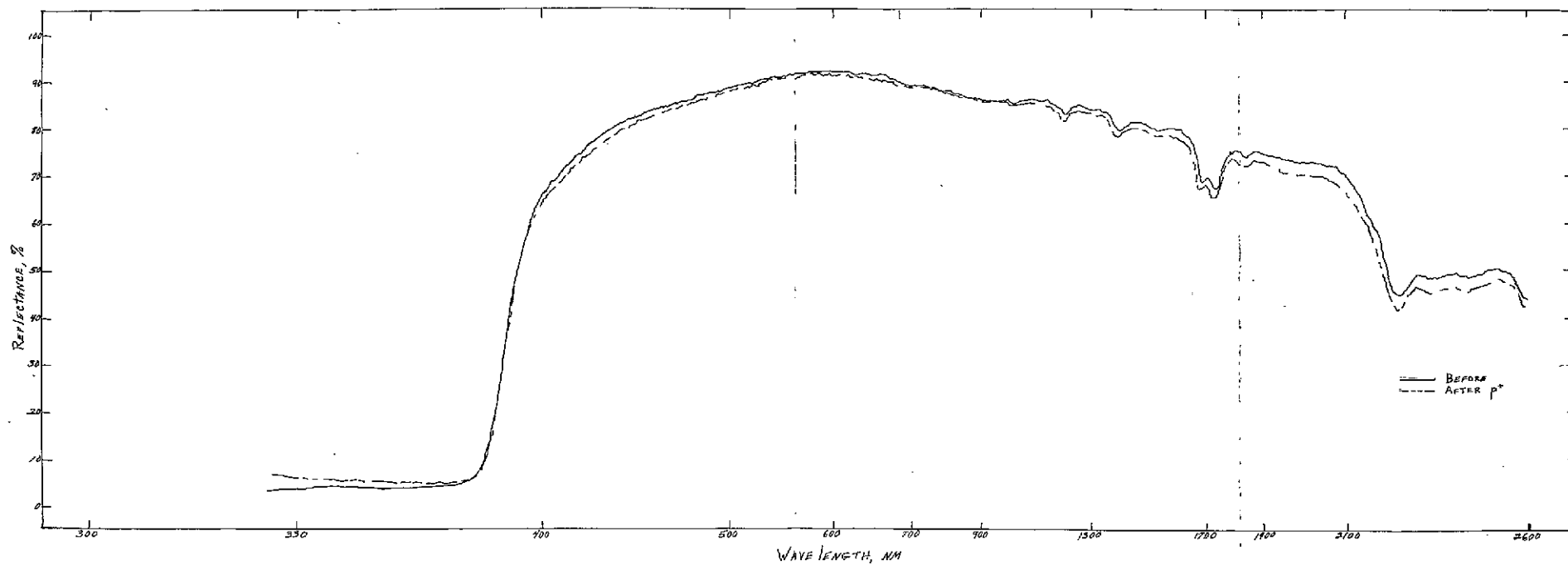


Figure 22 EFFECT OF 2.5×10^{15} PROTONS/CM² ON IN SITU
REFLECTANCE SPECTRA OF S-13G THERMAL-CONTROL PAINT

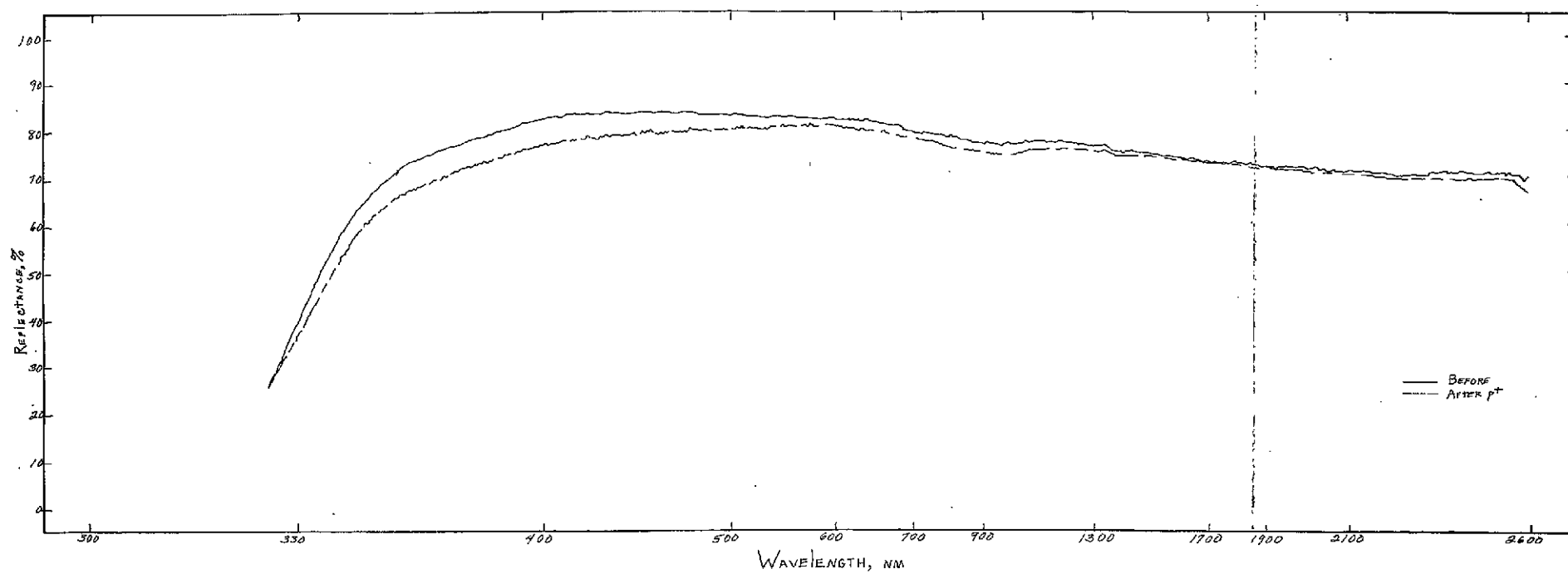


Figure 23 EFFECT OF 2.7×10^{15} PROTONS/CM² ON IN SITU REFLECTANCE SPECTRA OF PLASMA-CALCINED Zn₂TiO₄

FOLDOUT FRAME 1

FOLDOUT FRAME 2

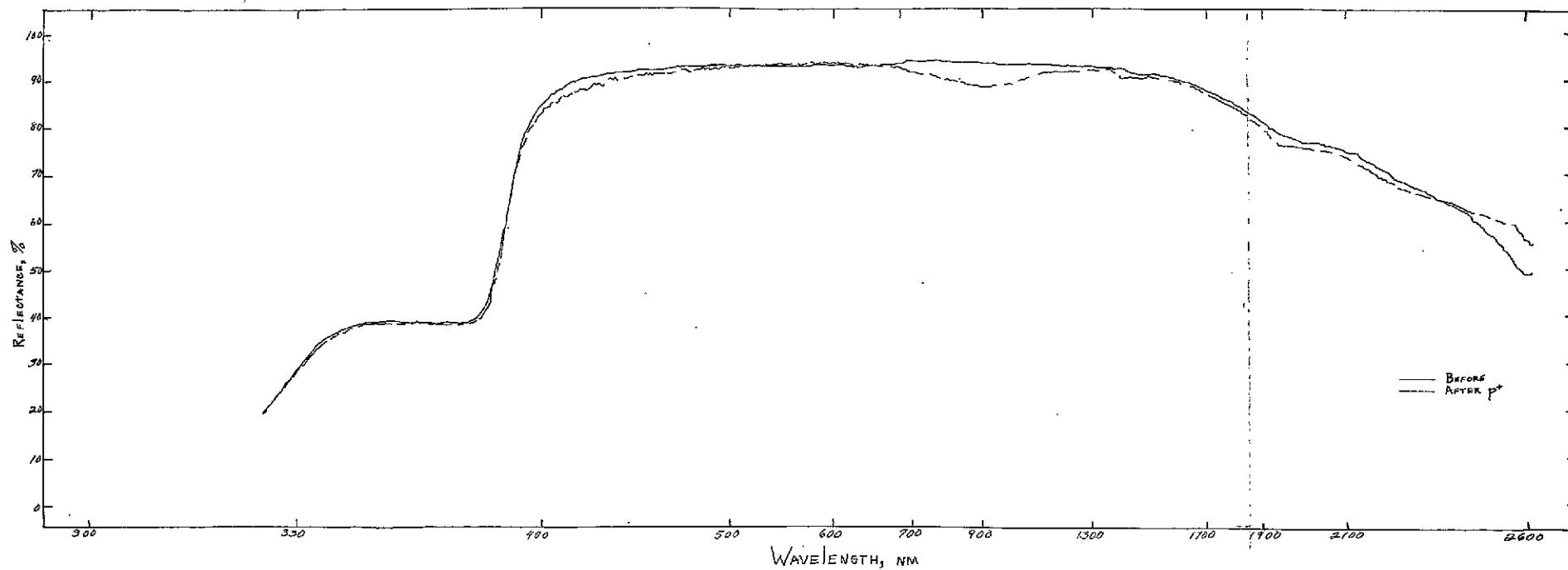


Figure 24 EFFECT OF 2.7×10^{15} PROTONS/CM² ON IN SITU REFLECTANCE SPECTRA OF PS7 PAINT PIGMENTED WITH ACID PHOSPHATE-TREATED Zn_2TiO_4

FOLDOUT FRAME 1

FOLDOUT FRAME 2

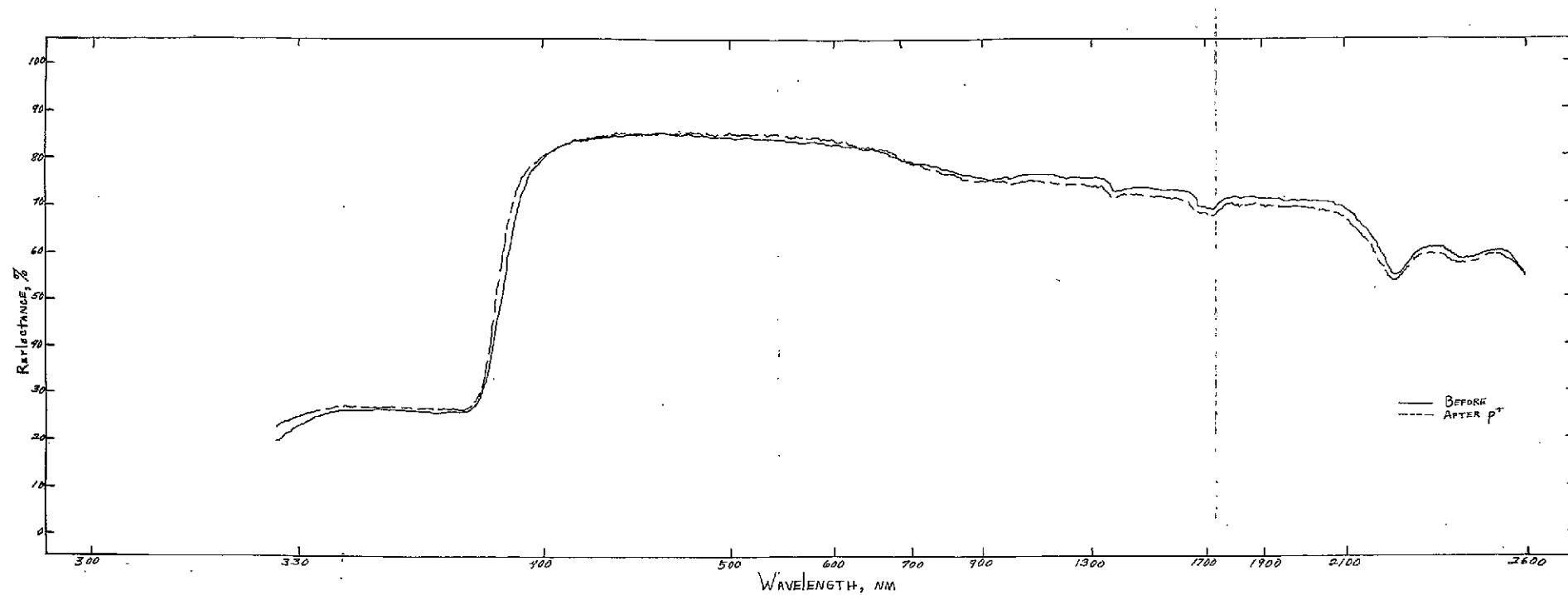


Figure 25 EFFECT OF 2.5×10^{15} PROTONS/CM² ON IN SITU REFLECTANCE SPECTRA OF OWENS ILLINOIS 650 (SILICONE) PAINT PIGMENTED WITH CYANATED Zn_2TiO_4

Table 1

SUMMARY OF PROTON-IRRADIATION DAMAGE

Figure	Material	Fluence 10^{15} p/cm ²	Flux 10^9 p/cm ² -sec	Proton Damage			
				Visable		IR	
				$\lambda_{\max}(\text{nm})$	$\Delta R(\%)$	$\lambda_{\max}(\text{nm})$	$\Delta R(\%)$
20*	SP500 ZnO	2.5	4.9	425	6.3	2500	6.0
21*	Z93	2.7	5.4	425	5.6	2500	4.0
22	S-13G (B-031)	2.5	4.9	450	1.5	2000	3.2
23	Zn ₂ TiO ₄ (Plasma)	2.7	5.4	400	5.7	950	2.0
24	Zn ₂ TiO ₄ (NaH ₂ PO ₄ - treated) in PS7	2.7	5.4	400	2.0	900	5.0
25	Zn ₂ TiO ₄ (Fe ⁺⁺ /Fe ⁺⁺⁺) in OI 650	2.5	4.9	None		2000	1.5

*Main target in each of two irradiations.

developed a mildly intense band at 900-nm wavelength and the powder specimen exhibited a much less intense band in that wavelength region. The Owens-Illinois 650-resin-based paint prepared from pigment that had been treated with ferric/ferrocyanide exhibited no specific damage at ~900-nm wavelength, but did degrade slightly in the entire infrared region.

C. Discussion

Although at this time it is impossible to correlate preparation and treatment parameters of the zinc orthotitanates with their proton-damage spectra, the behavior of the pure powders versus that of the silicone paints is intriguing. It may be that the binderless pigments are damaged physically by the proton irradiations and develop lattice-strain related damage similar to that attributed to grinding of zinc oxide. The explanation might then be that the pigments are physically protected by silicone binders from the "sand-blast" effects of the protons and that the threshold for damage to the silicone (ionization-wise) is greater than the threshold for development of a physically-induced B-band, as discussed previously by Gilligan (Ref. 9). (Current studies are devoted to increasing the total proton fluence deposited on the six specimens discussed herein.)

IV. CONCLUSIONS

Referring to the performance requirements, i.e., the proton flux, beam purity, beam energy, and energy spread and uniformity at the sample location, we have determined the important operational parameters affecting them. The most important parameter in regulating proton flux is the RF power applied and the vacuum pressure inside the system. The ion current out of the ion source is not a very strong function of voltage applied. Beam purity is primarily a function of the degree of separation and the angular geometrical constraints placed on the system. Beam energy is very well defined by the applied voltage at the probe. The energy spread is determined primarily on the basis of the number of lenses and the randomness imparted in the velocity distribution by any misalignment and nonuniform field potentials across the lenses. The einzel lenses help to correct this by achieving a fairly strong focus. The uniformity of the beam at the sample location is achieved principally by the quadrupole lenses and the application of a rather uniform electrical field which tends to spread the beam more than does the einzel. The beam at the sample location can be swept by using a saw-tooth generator or similar time-varying potential on the quadrupole lenses, thus achieving a better degree of uniformity. The characterization now is essentially complete.

Of prime importance in the characterization of this system is the assumption that the first peak in making a scan of current versus magnetic field strength is that the first peak is in fact the H^+ peak and succeeding peaks are due to H_2^+ or to other ionized species. We have calculated the magnetic field strength required to bend the proton beam 45° and have compared the calculated values with the actual numbers. We are quite certain that the first peak is, in fact, H^+ . The second peak is undoubtedly H_2^+ , probably with a slight amount of He^{++} . The third peak is He^+ , or other materials with similar charge-to-mass ratios. In the appendix we have indicated the calculations that were made

to substantiate the spectral location of the proton beam employed in the plot of ion current versus magnetic field strength. A number of calculations of the magnetic field required to bend the proton beam 45° were made for each of several different configurations of pole caps on the magnets. A representative calculation is shown in the Appendix.

REFERENCES

1. A.F. Sklensky, H.F. MacMillan, and S.A. Greenberg, "Solar-Radiation-Induced Damage to Optical Properties of ZnO-Type Pigments," Lockheed Missiles and Space Co. Report No. 4-17-68-1, Feb. '68.
2. G.A. Zerlaut, "Development of Space-Stable Thermal-Control Coating," IITRI Report No. U6002-51 (Triannual Report) Feb. 28, 1967.
3. G.A. Zerlaut, M. Marcour and G.A. Noble, "Development of Space-Stable Thermal Control Coatings," IITRI Report No. U6002-69 (Triannual Report), NASA Contract No. NAS8-5379, Oct. 25, 1968.
4. Zerlaut, G.A. and Courtney, W.J., "Space-Simulation Facility for In-Situ Reflectance Measurements," in Thermophysics of Spacecraft and Planetary Bodies, Vol. 20, Progress in Astronautics and Aeronautics, Heller, G. (ed.), Academic Press, New York, pp. 349-368, 1967.
5. Seitz, F., "On the Disordering of Solids by Action of Fast Massive Particles," Disc. Far. Soc. 5, pp. 271-282, 1949.
6. F.S. Johnson, "The Solar Constant" J. Meteor. 11, 431-39, 1954.
7. "Solar Electromagnetic Radiation," NASA SP-8005, National Aeronautics and Space Administration, June 1965.
8. E.N. Parker, "Interplanetary Dynamical Processes," Interscience Publishers, Inc., New York, N.Y., 1963.
9. Gilligan, J.E., "The Optical Properties Inducible in Zinc Oxide," in Thermophysics of Spacecraft and Planetary Bodies, Vol. 20, Progress in Astronautics and Aeronautics, Heller, G., (ed.) Academic Press, New York, 1967.

APPENDIX
CALCULATION OF BENDING

APPENDIX

CALCULATION OF BENDING

Using the magnetic field profiles measured with a gaussmeter, we must determine what magnetic field strength at the center will be required to bend the H^+ particles 45° . Let us use the equation

$$B = \frac{m v c}{e r}$$

repeatedly, breaking up the path into a series of lengths, each $1/2''$, and using the average B field for that length to be the value at the center of that length. This will underestimate the field by a small amount beyond the pole forces. Let us assume 1200 eV for the proton entering the field and start with $B = 337$ gauss at the center of the pole face, since that was the average determined empirically for a 48.5° bend. To determine the field at any point, we will multiply its value on the plot by $337/400$ or 0.82 , where 400 was the setting which produced this reading. Hence

$$r_{cm} = \frac{m v c}{e B} = \frac{5.12 \times 10^3}{B_{\text{gauss}}} .$$

The total angle for cup #5 is $48.5^\circ \pm 3.3^\circ$. The total angle, θ , for all 16 increments is

$$\theta = \sum_{i=1}^{16} 360^\circ \left(\frac{1}{2\pi r_i} \right) = 360^\circ (0.202) (0.963) = 50.4^\circ,$$

which is within the limits of cup #5.

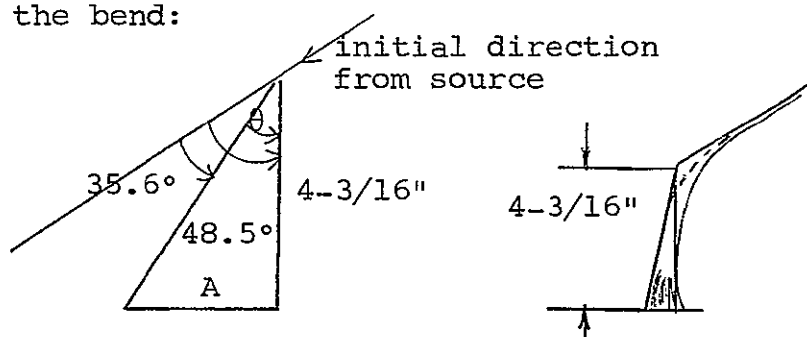
The difference is about 4% (or about 13 gauss); 324 gauss should be required. For a bend of 45° , the strength should be 300 gauss. The actual magnitude is about 275 gauss, and the difference may be because of slight energy losses in the plasma, effectively reducing the proton energy.

For H_2^+ , the radius will be $\sqrt{2}$ times that for H^+ in the same field. Therefore

$$\sum_{i=1}^{16} \frac{1}{r_{(H_2^+)}} = \frac{1}{\sqrt{2}} \sum_{i=1}^{16} \frac{1}{r_{(H^+)_i}} = \frac{0.693}{\sqrt{2}}$$

$$\text{Angle} = \frac{50.4^\circ}{\sqrt{2}} = 35.6^\circ$$

At $9/16''$ between cups and $4-3/16''$ from center of cup #5 to the center of the bend:



$$\tan \theta = \frac{A}{4-3/16''} = \tan(48.5 - 35.6)$$

$$A = \frac{67''}{16} \tan 12.9^\circ = \frac{67''}{16} (0.229) = 0.96''.$$

Therefore a $3/4''$ dia. hole will separate the two beams. The diameter of the hole in the first element of the second einzel is $0.496''$.

The peaks found on element #5 (48.5° bend) at a 1200-v probe voltage were $B_{H^+} = 330$ gauss and $B_{H_2^+} = 495$ gauss, with half-maximum points averaging 343 gauss ($300 + 385$) and 483 gauss (445 and 525).

Therefore H^+ and H_2^+ are supposed to be separated by $\sqrt{2} B_{H^+}$:

$$\text{peak } 330\sqrt{2} = 467, \text{ average } 343\sqrt{2} = 485.$$

At 2000 v, the peaks were found at $B_{H^+} = 448$ gauss and $B_{H_2^+} = 638$ gauss, with half maximum points at 420 gauss and 603 gauss. Therefore

$$\text{peak } 448\sqrt{2} = 634, \text{ average } 420\sqrt{2} = 595.$$

IIT RESEARCH INSTITUTE

The H^+ peak should change with probe voltage as \sqrt{V}

$$\sqrt{\frac{2000}{1200}} = 1.29$$

Therefore

peak 330(1.29) = 425, average 343(1.29) = 442
average 483(1.29) = 622, peak 495(1.29) = 638.

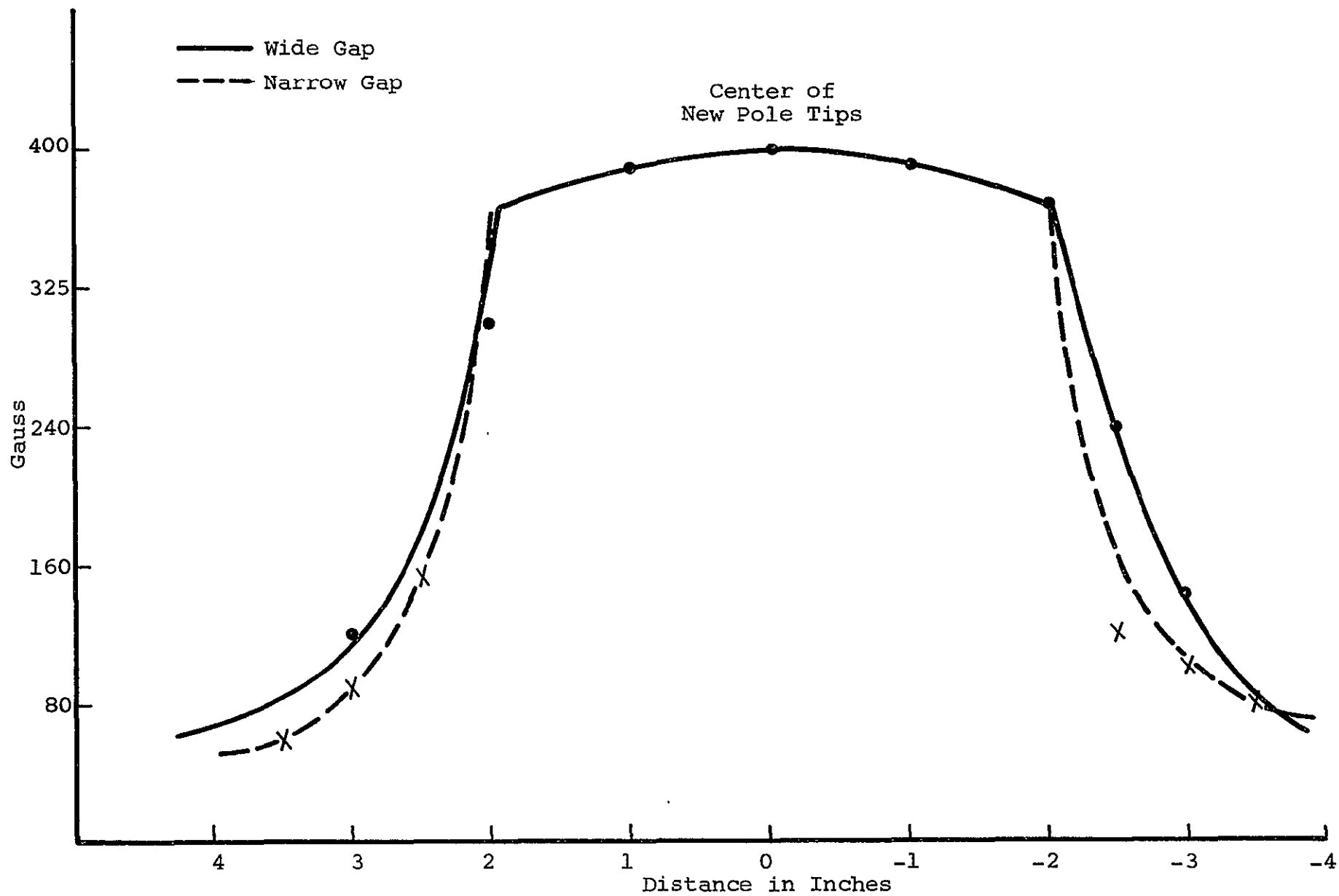


Figure A-1 MAGNETIC FIELD PROFILE